Liquid crystal dimers and the twist-bend nematic phase: on the role of spacers and terminal alkyl chains.

FORSYTH, E., PATERSON, D.A., CRUICKSHANK, E., STRACHAN, G.J., GORECKA, E., WALKER, R., STOREY, J.M.D. and IMRIE, C.T.

2020

Supplementary materials are appended after the main text of this document.

Liquid crystal dimers and the twist-bend nematic phase: On the role of spacers and terminal alkyl chains

Ewan Forsyth, Daniel A. Paterson[1], Ewan Cruickshank, Grant J. Strachan, Ewa Gorecka[2], Rebecca Walker, John M.D. Storey, Corrie T. Imrie *

Department of Chemistry, School of Natural and Computing Sciences, University of Aberdeen, Meston Building, Aberdeen AB24 3UE, UK.

Present address:

[1] School of Physics and Astronomy, and School of Chemistry, University of Leeds, Leeds, UK.

[2] Department of Chemistry, University of Warsaw, ul. Zwirki i Wigury 101, 02-089 Warsaw, Poland.

* Corresponding author: C.T. Imrie. E-mail address: c.t.imrie@abdn.ac.uk

ABSTRACT

The synthesis and characterisation of four series of liquid crystal dimers based on benzylideneaniline mesogenic units, and in which the lengths of terminal alkyloxy chains are varied are reported. The series differ in terms of their flexible spacers, namely, heptamethylene, nonamethylene, hexyloxy, and oxypentyloxy chains. The heptamethylene- and nonamethylene-linked dimers both show conventional nematic, N, and twist-bend nematic, N_{TB}, phases with short terminal chains, and smectic behaviour emerges on increasing terminal chain length. This is attributed to increased molecular inhomogeneity driving microphase separation. The dimers containing the shorter heptamethylene spacer show a smectic A phase whereas those with the longer nonamethylene spacer exhibit an anticlinic smectic C phase. Smectic behaviour is not observed for the dimers containing either a hexyloxy spacer which exhibit nematic and twist-bend nematic phases, or with an oxypentyloxy spacer which show only a conventional nematic phase. A general observation is that T_{NTBN} and T_{NI} alternate in the same sense in a homologous series on varying the length of the terminal alkyl chains suggesting that the spatial uniformity of the molecular curvature is an important factor in stabilising the N_{TB} phase. The transitional properties of the four corresponding dimers possessing nitrile terminal substituents are also described. These show enantiotropic nematic phases, and in addition, for those containing either polymethylene or hexyloxy spacers, a twist-bend nematic phase is observed. Differences in the thermal behaviour of the dimers may be attributed largely to changes in molecular shape arising from the nature of the link between the spacer and mesogenic units.

Keywords: Twist-bend nematic, Dimer, Terminal chain, Smectic phase

1. Introduction

The discovery of the twist-bend nematic, N_{TB}, phase was now almost a decade ago [1] but this intriguing phase remains at the forefront of liquid crystal research across the globe. This discovery confirmed earlier independent predictions made by Meyer [2] and Dozov [3]. At the root of Dozov's seminal study was the assertion that bent molecules have a strong natural tendency to pack into bent structures but that pure uniform bend in space is not allowed. He predicted that to accommodate this, the directors must show other local deformations, namely twist or splay. In the twist-bend nematic phase, the director forms a heliconical structure in which it is tilted with respect to the helical axis. Chirality occurs spontaneously in this phase and so equal numbers of the degenerate left- and right-handed helices are formed. The pitch length in the N_{TB} phase is strikingly small and typically just 3–4 molecular lengths [4]. If the constituent molecules are chiral this removes the degeneracy of the left- and right-handed helices and the chiral twist-bend nematic phase is observed [5]. The N_{TB} phase is normally observed on cooling a conventional nematic phase, but examples of direct N_{TB}-isotropic transitions have been reported in pure compounds [6,7] and in mixtures [8]. Aside from their considerable fundamental interest, materials that exhibit the N_{TB} phase have also been shown to have significant application potential in wide-ranging technologies such as tuneable lasers and smart windows [9–13] and photoswitchable adhesives [14].

A major area of ongoing activity involves establishing and understanding the relationships between molecular structure and the observation of the N_{TB} phase. This is work still very much in progress but it is widely believed that molecular curvature is a prerequisite to the observation of the N_{TB} phase and this may be understood within the framework of Dozov's prediction [3]. The overwhelming majority of twist-bend nematogens may be described as odd-membered dimers in which two mesogenic units are connected via a flexible spacer containing an odd number of linking atoms which ensures that, on average, the molecular structure is bent [15,16]. The extent of this molecular curvature is governed to a large extent by the nature of the links between the spacer and the mesogenic units, and the length of the spacer. A wide range of differing structures have been characterised to explore this relationship [17–26]. In order to manipulate the transition temperatures in these systems considerable effort has also been invested in varying the nature of mesogenic units and terminal substituents [27–33]. Although the majority of twist bend nematogens are odd-membered dimers, others structures have also been shown to support the formation of the N_{TB} phase including higher oligomers [34–38], semi-rigid bent core liquid crystals [39,4] and hydrogen-bonded supramolecular systems [41–46]. In each of these, however, molecular curvature appears to be the critical structural feature.

By comparison, far less attention has been afforded to the effects of increasing terminal chain length on the formation of the N_{TB} phase in either odd-membered symmetric [6,47,48] or nonsymmetric dimers [49,5]. The latter studies underpinned the discovery of the heliconical smectic phases [51,52] that had also been predicted by Dozov in his seminal work [3]. In order to better understand the role of the terminal chain in determining the liquid crystal behaviour of these bent molecules, we report here the transitional properties of four new series of materials in which the lengths of the terminal chains are varied, see Fig. 1. These four series are each based around a differing spacer, and to compare the role of the spacers, we first discuss the transitional properties of the four cyanobenzylideneaniline-based dimers, CN-7-CN, CN6O-CN, CN-O5O-CN and CN-9-CN. In each of these acronyms, the dash refers to the benzylideneaniline unit, CN to the nitrile group, the number indicates the number of carbon atoms in the spacer, and O represents an ether link. The heptyl (7), hexyloxy (6O) and oxypentyloxy (O5O) spacers were selected to keep the spacer length constant while varying the shape of the molecule. The nonyl (9) spacer allowed for the effect of spacer length to be considered. We then move to the main focus of the paper and describe the dependence of the

transitional behaviour on the length of the terminal alkyloxy chains in the four series *m*O-7-O*m*, *m*O-6O-O*m*, *m*O-O5O-O*m*, and *m*O-9-O*m*. In each of these acronyms m refers to the number of carbon atoms. in the terminal chains

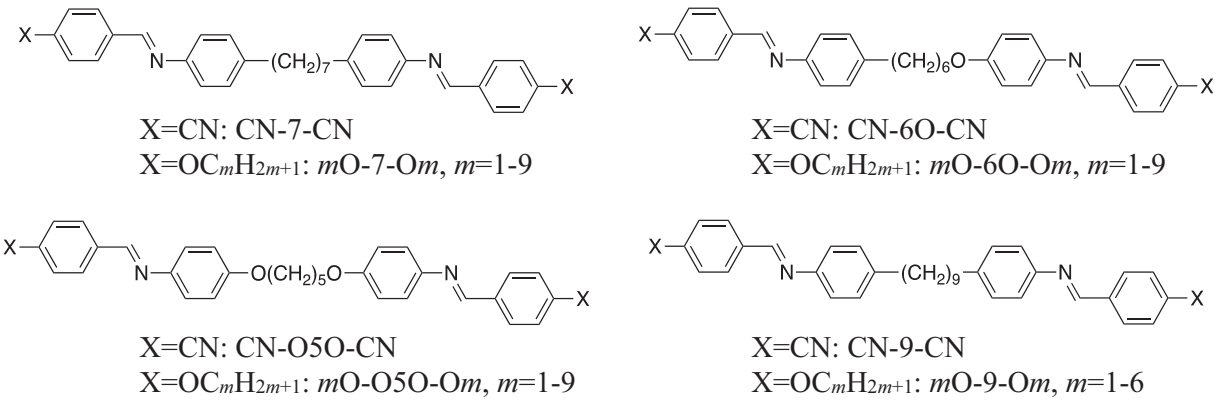

Fig. 1. The structures of the dimers and the acronyms used to refer to them.

2. Experimental

2.1. Synthesis

The target dimers were obtained by the reaction of either 1,5-bis(4-aminophenyl-4′-oxy)pentane, 1-(4-aminophenoxy)-6-(4-aminophenyl) hexane, or an α,ω-bis(4-aminophenyl-4′-)alkane with the appropriate 4-substitutedbenzaldehyde under conditions described in detail elsewhere [53]. The preparation of 1,5-bis(4-aminophenyl-4′-oxy)pentane followed the procedure described by Henderson et al. [54]. At the outset of this study, the α,ω-bis(4-aminophenyl-4′-)alkanes were prepared using a method described in the literature [55] but in order to improve yields the route shown in Scheme 1(a) was developed and adopted. 1-(4-Aminophenoxy)-6-(4-aminophenyl)hexane was obtained using the route shown in Scheme 1(b). Detailed descriptions of the synthesis and characterisation of all the final products and their intermediates are provided in the ESI.

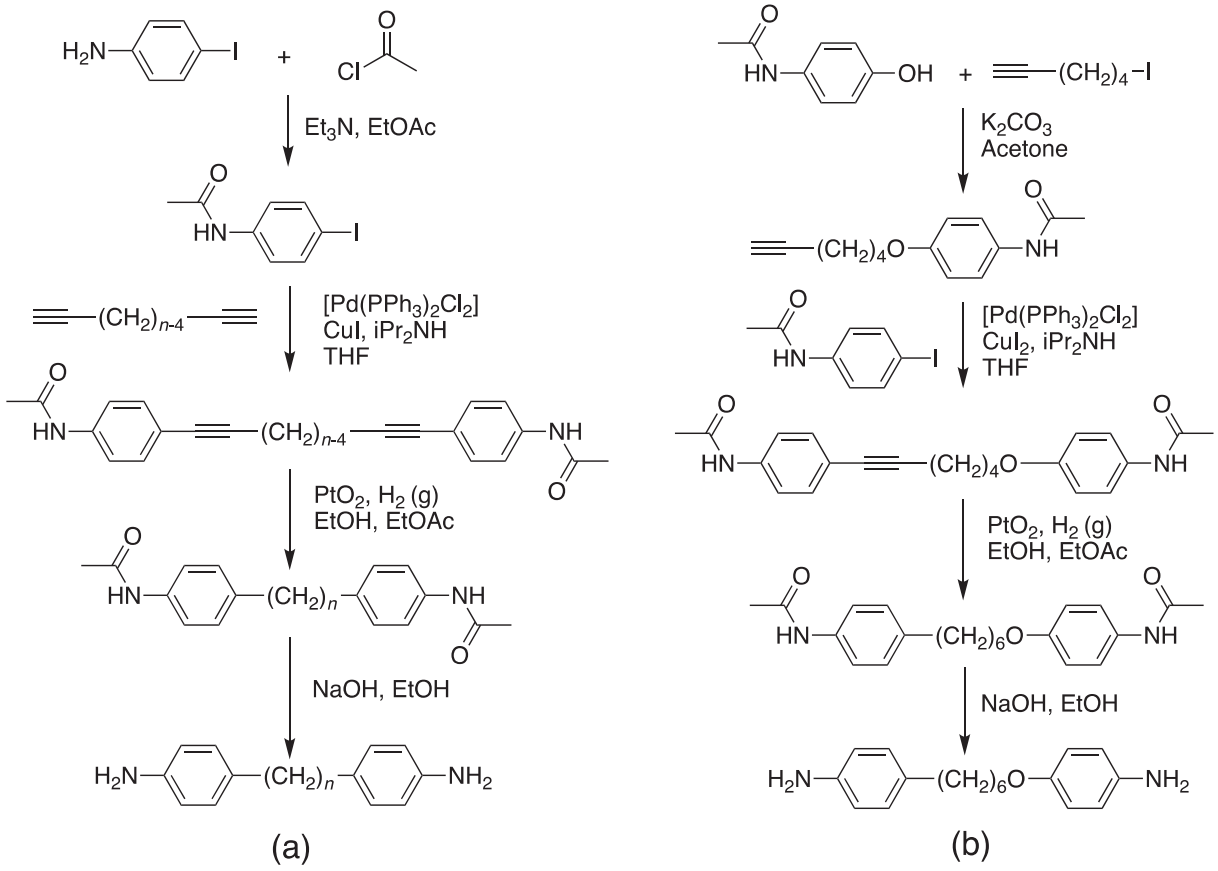

Scheme 1. The synthetic routes used to obtain (a) the α,ω-bis(4-aminophenyl-4′-)alkanes, and (b) 1-(4-aminophenoxy)-6-(4-aminophenyl)hexane.

2.2. Thermal characterisation

The transitional properties of the dimers were determined using differential scanning calorimetry using a Mettler Toledo DSC3 differential scanning calorimeter equipped with a TSO 801RO sample robot. Calibration was performed using indium and zinc as standards. Heating and cooling rates were 10 °C min^{-1} and all samples were measured under a nitrogen atmosphere. Transition temperatures and associated enthalpy changes were extracted from heating traces unless otherwise noted. For each sample, two aliquots were measured, and the data listed are the averages of the sets of data. Phase identification was performed using polarised light microscopy using an Olympus BH2 polarising optical microscope equipped with a Linkam TMS 92 hot stage. All optical textures have been obtained using untreated glass slides unless stated otherwise. X-ray diffractograms were obtained with a Bruker D8 GADDS system (CuKα line, Goebel mirror, point beam collimator, VANTEC2000 area detector).

2.3. Molecular modelling

Geometry optimisation was carried out using DFT calculations at the B3LYP 6-31G(d) level of theory with Gaussian09 software [56]. Space filling models were generated from the optimised geometries using the QuteMol package [57]. Although ether-linked spacers have been found to have a *gauche* linkage in their lowest energy state [19], the energy difference between this and the all-*trans* conformation is small (ca 1 kJ mol^{-1}) and it is expected that the greater linearity of the all-*trans* state will be more favourable within a liquid crystalline phase [58]. Based on this, the geometry optimisations were carried out with the central spacer in the all-*trans* conformation. This assumption is in accord with similar studies [21].

3. Results and discussion

Phase identification was performed using polarised light microscopy on the basis of the observation of characteristic optical textures. Thus, for nematic, N, phases a schlieren texture was observed containing both two- and four-point singularities, and which flashed when subjected to mechanical stress. A representative nematic schlieren texture is shown in Fig. 2. The entropy changes associated with these transitions are wholly consistent with the assignment [59,60]. On cooling the nematic phase for a number of these dimers, textures developed containing regions of blocky and striped texture and parabolic and rope-like defects, see Fig. 3. These features are characteristic of the twist-bend nematic, N_{TB}, phase. In addition, the op cal flickering apparent in the nema c schlieren texture associated with director fluctua ons froze at the N_{TB}-N transition. Members of the mO-7-Om series exhibited the smectic A, SmA, phase assigned on the basis of the observation of a focal conic fan texture in coexistence with regions of homeotropic alignment, see Fig. 4. 5O-9-O5 and 6O-9-O6 show a smectic C phase for which coexisting regions of focal conic fan and schlieren texture containing both four- but predominantly two-point brushes were observed, see Fig. 5(a) and (b). Two-brush defects are characteristic of the smectic CA phase in which the mesogenic units are arranged in an an clinic fashion. This view is supported by the smooth and blemish-free focalconic domains that indicate an absence of tilted domains. The phase assignment was confirmed using X-ray diffrac on and Fig. 6 shows the patern obtained for the smectic C phase exhibited by 6O-9-O6. This contains a sharp low-angle signal and a less intense second harmonic indicating a layered structure, and a diffuse wide-angle reflec on characteris c of a liquid-like arrangement of the molecules within a layer. The smectic layer spacing is 22.3 Å, and corresponds to approximately half the molecular length, l, estimated to be 43 Å. This implies an intercalated arrangement of the molecules in the SmC_A phase and we will return to this observation later. On cooling, the schlieren texture became mosaic-like and contained needles, Fig. 5(c), and the focal conic fans developed blemishes becoming

less well-defined, Fig. 5(d). These changes indicate an increase in in-plane ordering and strongly suggest the lower temperature phase is a highly ordered smectic or soft crystal phase. The entropy change associated with the transition is consistent with this view [61]. The X-ray pattern obtained for this phase is also shown in Fig. 6, and the wide-angle signal has narrowed and partially split into a number of peaks consistent with a highly ordered phase. There are off axis signals in the low angle region implying that this is not a lamellar structure. In the small angle region, a strong signal corresponding to the full molecular length, *l*, is apparent suggesting that the main packing pattern in the crystal is a molecular arrangement with side to side position of molecules and with *d* = *l*. We have designated this phase as CrX.

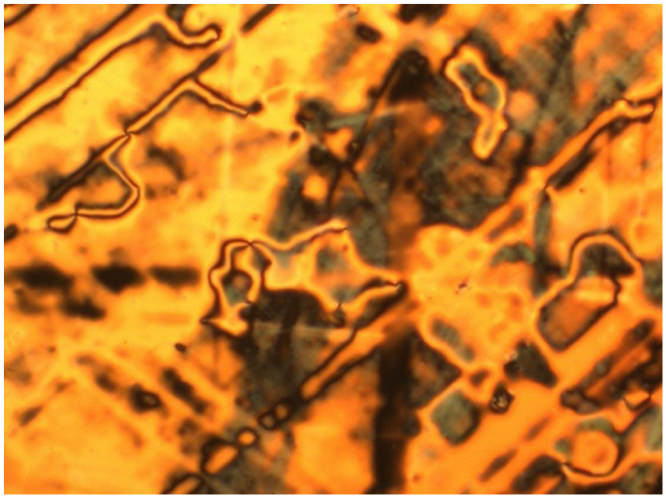

Fig. 2. The schlieren texture of the nematic phase shown by 2O-O5O-O2 ($T = 198$ °C).

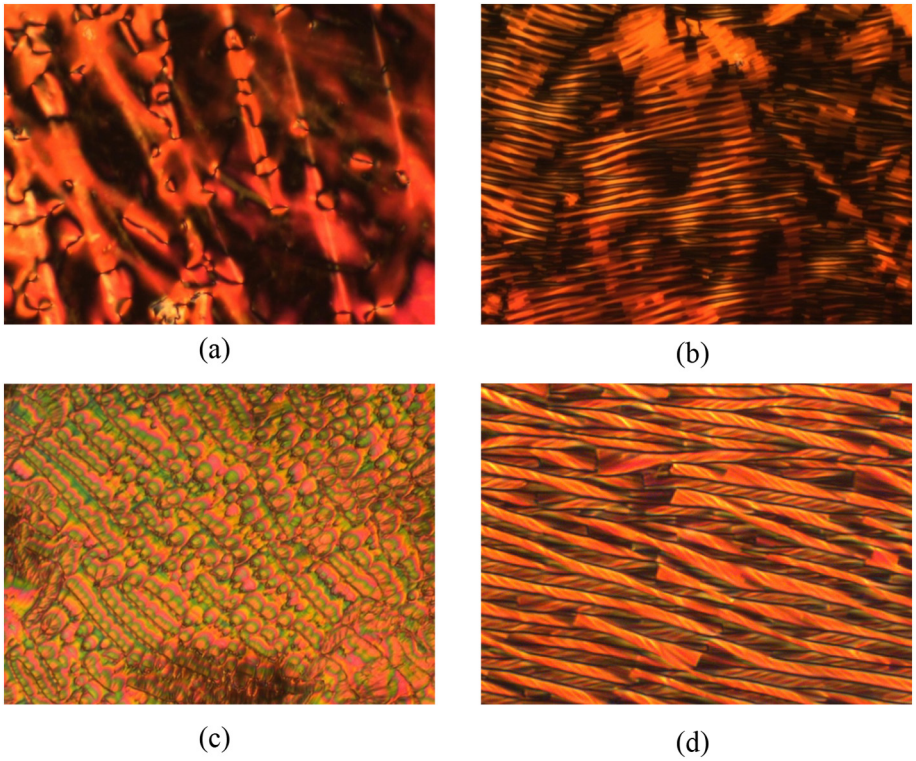

Fig. 3. The optical textures exhibited by 2O-9-O2 on cooling from the isotropic phase: (a) the nematic schlieren texture ($T = 139$ °C); (b) the striped, blocky texture ($T = 101$ °C) and (c) parabolic defects (101 °C) seen for the N_{TB} phase. (d) The characteristic rope-like texture observed for the N_{TB} phase shown by 2O-7-O2 ($T = 114$ °C).

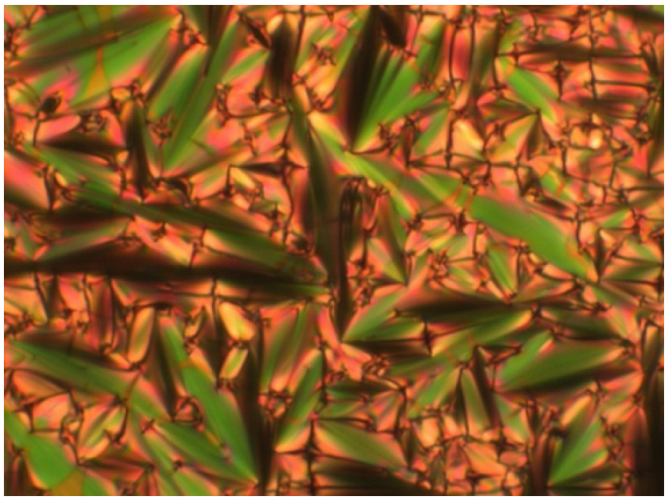

Fig. 4. The focal conic fan texture of the smectic A phase shown by 5O-7-O5 ($T = 110$ °C).

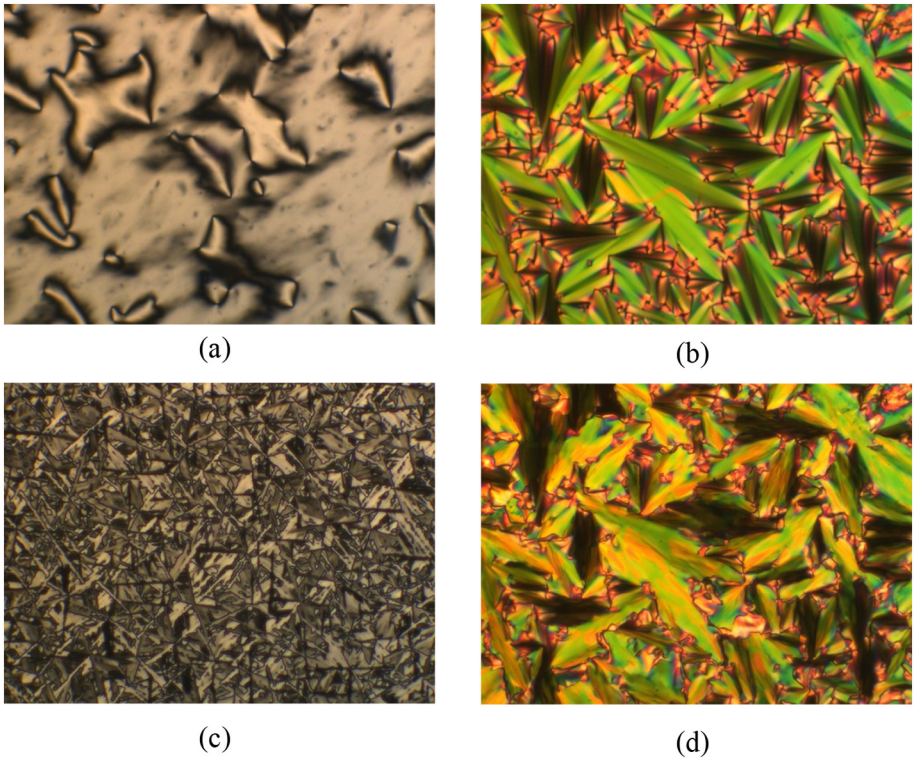

Fig. 5. The optical textures seen for 6O-9-O6 on cooling from the isotropic phase: (a) the schlieren ($T = 116$ °C) and (b) coexisting focal conic fan textures ($T = 109$ °C) seen for the SmC phase; (c) the mosaic-like texture containing needles ($T = 108$ °C), and the coexisting focal conic fans with blemishes ($T = 102$ °C) observed for the CrX phase.

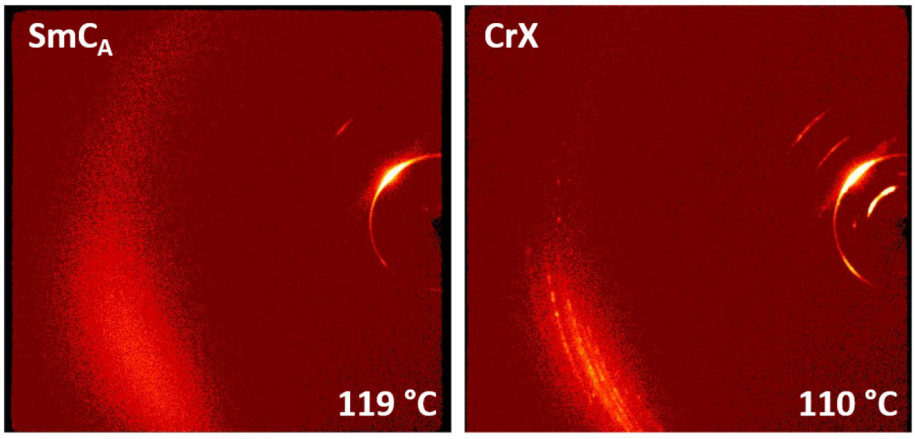

Fig. 6. X-ray diffraction patterns of 6O-9-O6 in the SmC_A (left) and CrX (right) phases.

Table 1 lists the transitional properties of the four cyano-terminated dimers and for comparative purposes, data for CN-5-CN are also listed [2,55]. Each new dimer shows an enantiotropic, conventional nematic phase, and with the exception of CN-O5O-CN, a twist-bend nematic phase. If we first consider the effects of increasing the spacer length, we see that the melting point falls whereas both T_{NTBN} and T_{NI} increase.

Similar trends are observed for the corresponding cyanobiphenyl-based dimers containing the same spacers, see Table 2 [18,19]. The decrease in melting point may be attributed to the increased flexibility of the spacer. For the corresponding dimers containing 4-phenyl 4'-cyanobenzoate mesogenic units, an increase in the melting point occurs on moving from the heptyl to nonyl homologue, see Table 3 [62,63]. We note, however, that like transitions are not always being compared. The CBnCB series tend to show the lowest melting point and the 4-phenyl 4'-cyanobenzoate-based dimers the highest. This may reflect stronger lateral dipolar interactions in the ester-linked materials.

The CN-*n*-CN series shows the highest, and the CBnCB series the lowest values of T_{NTBN} and T_{NI} for any given value of n. The increase in T_{NI} is always greater than that in T_{NTBN} on extending the mesogenic units. The increase in T_{NTBN} on increasing the length of the mesogenic units suggests that this structural change enhances the molecular curvature whereas the higher values of T_{NI} arise from the stronger interactions between the extended mesogenic units. The latter is the larger of the two effects, and in consequence the relative stability of the N_{TB} to N phase, as measured by the ratio T_{NTBN}/ T_{NI} , is largest for the CBnCB series and smallest for the CN-n-CN series. The more significant increase in T_{NI} than in T_{NTBN} on increasing the leng th of the mesog enic units may be atributed to the interaction between the orientational ordering of the nematic phase and the director. This will influence the conformational distribution of the molecules and calculations hav e shown that for a methylene-linked dimer in the nematic phase more elongated conformers are favoured [19]. This will serve to reduce T_{NTBN} by counteracting the anticipated increase in molecular curvature arising from the more anisometric mesogenic units. The value of T_{NTBN} for CN-7-CN is 4 °C higher than that of the corresponding 4-phenyl 4'-cyanobenzoate-based dimer whereas TNI is some 15 °C higher. For the nonyl homologues, the differences in T_{NTBN} and T_{NI} are 10.4 °C and 10.5 °C, respectively. This reflects a fall in T_{NTBN} on passing from the heptyl to nonyl members of the 4-phenyl 4'-cyanobenzoate-based

Table 1
The transitional properties of the cyano-terminated dimers containing benzylideneaniline fragments. Data for CN-5-CN have been extracted from the literature [20,55].

Dimer	T_{Cr}/°C	$T_{N_{TB}N}$/°C	T_{NI}/°C	$\Delta S_{Cr}/R$	$\Delta S_{N_{TB}N}/R$	$\Delta S_{NI}/R$
CN-5-CN	147	113	125	9.7	0.16	0.13
CN-7-CN	127	124[a]	154	10.08	0.11[a]	0.22
CN-9-CN	122	125[a]	157	1.06	0.05[a]	0.38
CN-6O-CN	147	120[a]	193	12.34	0.04[a]	0.50
CN-O5O-CN	176		222	14.65		0.71

[a] Denotes values taken on cooling traces of DSC.

Table 2
The transitional properties of dimers containing cyanobiphenyl mesogenic units [18,19].

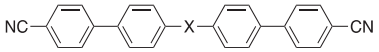

X	Dimer	T_{Cr}/°C	$T_{N_{TB}N}$/°C	T_{NI}/°C	$\Delta S_{N_{TB}N}/R$	$\Delta S_{NI}/R$
$(CH_2)_5$	CB5CB	150	92	97	0.47	0.13
$(CH_2)_7$	CB7CB	102	103	114	0.27	0.22
$(CH_2)_9$	CB9CB	86	108	124	0.08	0.33
$(CH_2)_6O$	CB6OCB	99	109	155	0.01	0.48
$O(CH_2)_5O$	CBO5OCB	139	79	187		0.75

Table 3
The transitional properties of dimers containing 4-phenyl 4′-cyanobenzoate mesogenic units [62,63].

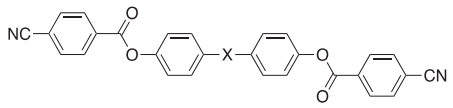

X	T_{Cr}/°C	$T_{N_{TB}N}$/°C	T_{NI}/°C	$\Delta S_{N_{TB}N}/R$	$\Delta S_{NI}/R$
$(CH_2)_7$	149	120	139	0.06	0.19
$(CH_2)_9$	157.6	114.5	146.6	0.20	0.43
$O(CH_2)_5O$	166.6	96.8	189.2		0.96

series but an increase in the biphenyland benzylideneaniline-based series. The physical significance of this difference in behaviour is not immediately apparent. The scaled entropy change associated with the N-I transition, $\Delta S_{NI}/R$, are very similar for the corresponding members in each series. In contrast, the values of $\Delta S_{NTBN}/R$ differ but this may be accounted for in terms of the temperature range of the preceding nematic phase [18].

We now turn our attention to the effects of changing the nature of the spacer while keeping its length constant by comparing the behaviour of CN-7-CN, CN-6O-CN and CN-O5O-CN. The melting point increases each time a methylene group is replaced by an oxygen atom. This may be understood in terms of the accompanying structural change and specifically, the bond angle between the para axis of the mesogenic unit and the first bond in the spacer. For a methylene link this angle is 113.5° whereas for an ether link it is 126.4°. This larger angle makes the all-trans conformation of an ether-linked dimer more linear than that of a methylene-linked dimer, see Fig. 7. It is clear that the curvature of the dimer containing a hexyloxy spacer is intermediate between those of the symmetric dimers. The higher melting points of the ether-linked dimers may be attributed to the greater linearity of these allowing for greater packing efficiency in the crystal phase, as well as enhanced polar interactions arising from the ether links. This particular trend is not observed for the biphenyl-based dimers, for which the melting point of CB6OCB is slightly lower than that of CB7CB but that of CBO5OCB is considerably higher.

The value of T_{NI} increases by 39 °C on passing from CN-7-CN to CN6O-CN and a further 29 °C for CN-O5O-CN. These increases may be atributed to the change in molecular shape described earlier and shown in Fig. 7. It is also evident that $\Delta S_{NI}/R$ also increases on replacing a methylene unit by an oxygen atom, see Table 1. Both these trends are also observed for the corresponding biphenyl-based materials, see Table 2, and for the methylene- and ether-linked 4-phenyl 4′-cyanobenzoate-based dimers although it is surprising that T_{NI} for the later is not somewhat higher, see Table 3. These

changes in T_{NI} and $\Delta S_{NI}/R$ are completely in accord with predictions of a theoretical model developed by Luckhurst and co-workers in which the only difference between the dimers considered are the bond angles between the para axis of the mesogenic unit and the first bond in the spacer [64–66]. Within the framework of the model, increases in T_{NI} and $\Delta S_{NI}/R$ may be accounted for solely in terms of this geometrical factor.

The value of T_{NTBN} shown by CN-6O-CN is lower by 4 °C than that seen for CN-7-CN. On the basis of the previous discussion, CN-6O-CN is expected to be more linear than CN-7-CN, and given that the N_{TB}-N transition is predominantly shape driven, it may be expected that CN7-CN should exhibit the higher value of T_{NTBN}. However, this is not the case for the corresponding cyanobiphenyl-based dimers. CB6OCB shows a value of T_{NTBN} 6 °C higher than that of CB7CB, see Table 2, and this difference is larger for shorter spacers such that T_{NTBN} is 11 °C higher for CB4OCB than for CB5CB. Increasing the spacer length, however, reduces the difference in T_{NTBN} such that the values for CB8OCB and CB9CB are similar [18,67] and CB10OCB actually shows a lower T_{NTBN} than CB11CB [18]. To account for these observations, it was suggested that for shorter spacer lengths the more linear ether-l inked fragment in the CBnOCB series promotes the local packing of the molecules in the N_{TB} phase. On increasing spacer length this effect is diluted by the greater number of conformations available to the spacer, and now the more pronounced curvature of the CBnCB series, critical in determining the bend elastic constant [68], becomes the dominant factor in determining T_{NTBN} [18]. For any given series, this cross-over in behaviour may be expected to depend, at least in part, on the shapes of the mesogenic units and how these contribute to the overall molecular shape. As these units become more anisometric, the difficulty associated with packing these nonsymmetric molecules increases, and T_{NTBN} falls relative to T_{NI}. Thus, T_{NTBN} for CB6OCB is greater than that for CB7CB and local packing considerations reinforce the local intercalation of the molecules overturning the order predicted on shape alone, whereas T_{NTBN} for CN-7-CN is greater than that of CN-6O-CN as would be predicted from their relative molecular curvatures, see Fig. 7.

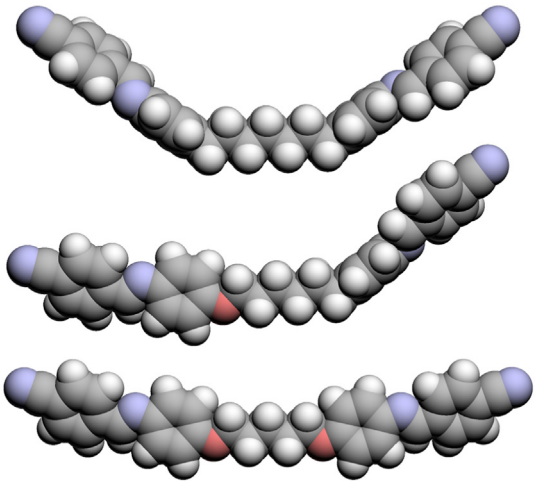

Fig. 7. Space filling models for CN-7-CN (top), CN-6O-CN (middle) and CN-O5O-CN (bottom).

We now consider the effects of increasing the length of the terminal chains, and the transitional properties of the *m*O-7-O*m* series are listed in Table 4. The dependence of their transition temperatures on the length of the terminal chains, *m*, is shown in Fig. 8. The first four members of the series exhibit a conventional nematic phase, and the first two also show the twist-bend nematic phase. A smectic A phase emerges with the fourth member, and for *m* = 5–7, a direct smectic A-isotropic transition is observed. The octyl and nonyl members do not show liquid crystalline behaviour presumably because of the rather monotropic nature of these materials. The clearing temperatures initially show a pronounced alternation in which 2O-7-O2 shows the highest value, and this quickly attenuates on increasing *m*. The value of T_{NTBN} increases in a similar fashion to T_{NI} on moving from 1O-7-O1 to 2O-7-O2 and must fall equally dramatically on passing to 3O-7-O3 for which an N_{TB} phase was not observed. We will discuss the physical significance of these observations later. The emergence of smectic behaviour for 4O7-O4 is consistent with the very general observation that for smectic behaviour to be observed in symmetric dimers the combined lengths of the terminal chains has to exceed that of the spacer [61,69]. This structure-property relationship has been attributed to the nature of the interaction between the spacer and terminal chains and thought to indicate that this is unfavourable [61] and inhibits the formation of an intercalated smectic phase in which the spacer and terminal chains are required to mix [70,71]. Instead, a monolayer smectic phase is typically observed for this class of materials, the formation of which is driven by the increased molecular inhomogeneity arising from the long terminal alkyl chain. For this to occur for a symmetric dimer the length of a terminal chain must exceed half that of the spacer.

Table 4.
The transitional propterties of the *m*0-7-0*m* series.

m	T_{Cr}/°C	T_{SmA-}/°C	$T_{N_{TB}N}$/°C	T_{NI}/°C	$\Delta S_{Cr}/R$	$\Delta S_{N_{TB}N}/R$	$\Delta S_{NI}/R$ [a]$\Delta S_{SmI}/R$
1	112		87*	104*	13.38	0.12*	0.11*
2	109		114	131	12.40	0.07	0.22
3	112			102†	9.88		
4	111	107†		109*	10.11		0.11*
5	113	110†			6.50		0.28[a]
6	121	116†			4.12		
7	118	112†			10.51		
8	120				7.85		
9	119				7.74		

* Denotes values taken on cooling traces of DSC.
† Denotes values from POM.

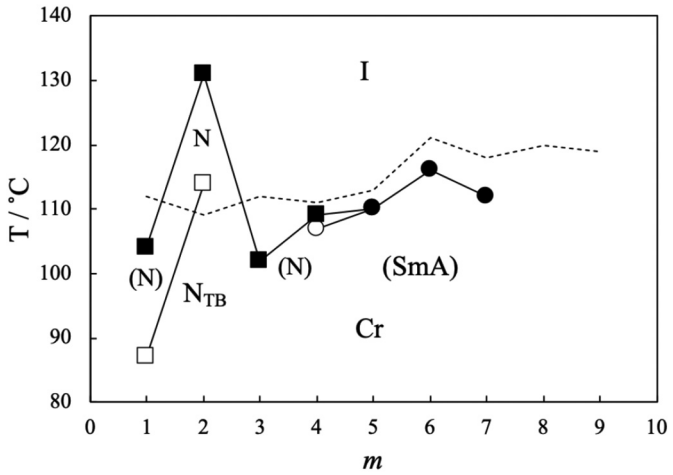

Fig. 8. The dependence of the transition temperatures on the length of the terminal chains, *m*, for the *m*O-7-O*m* series. The broken line connects the melting points, open squares indicate N-N_{TB} transitions, filled squares N-I transitions, open circles SmA-N transitions and filled circles SmA-I transitions

The transitional properties of the *m*O-9-O*m* series are listed in Table 5, and all six members show enantiotropic phase behaviour as seen in Fig. 9. This reflects the combination of lower melting points and higher clearing temperatures than seen for the corresponding members of the *m*O-7-O*m* series, which as we have seen, with the exception of 2O-7-O2, are monotropic in nature. The lower melting points of the *m*O-9-O*m* series may be attributed to the entropic contribution arising from the increase in flexibility of the spacer. The higher values of T_{NI} seen for the *m*O-9-O*m* series may also be attributed to the greater flexibility of the longer spacer, and the larger number of conformations available to the spacer to adopt more linear conformations so enhancing T_{NI}.

Table 5
The transitional properties of the *m*O-9-O*m* series.

m	T_{Cr}/°C	T_{CrXSmC}/°C	T_{SmC-}/°C	$T_{N_{TB}N}$/°C	T_{NI}/°C	$\Delta S_{Cr}/R$	$\Delta S_{CrXSmC}/R$	$\Delta S_{SmC-}/R$	$\Delta S_{N_{TB}N}/R$	$\Delta S_{NI}/R$
1	105			102[a]	127[a]	12.02			0.04[a]	0.25[a]
2	103			117	138	9.04			0.05	0.41
3	104			95[b]	112	11.96				0.20
4	104			104[a]	120	11.39			0.04	0.31
5	84		105[b]		110[a]	5.23				0.20[a]
6	83	110	119			6.55	3.20	4.32		

[a] Denotes values taken on cooling traces of DSC.
[b] Denotes values from POM.

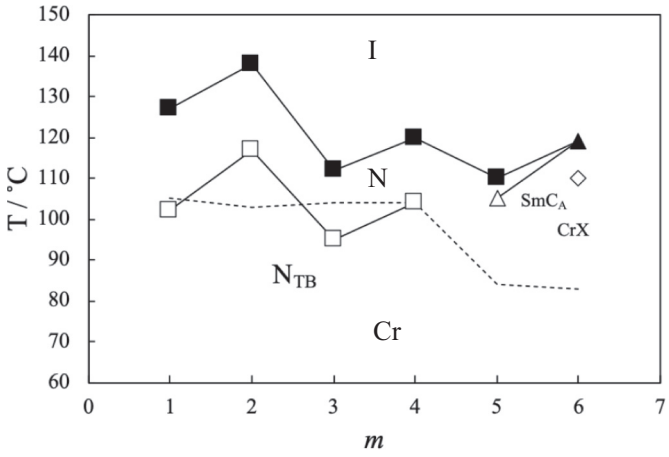

Fig. 9. The dependence of the transition temperatures on the length of the terminal chains, m, for the mO-9-Om series. The broken line connects the melting points, open squares indicate N-NTB transitions, filled squares N-I transitions, open triangles SmCA-N transitions, filled triangles SmCA-I transitions and the open diamond a CrX-SmCA transition.

The first four members of the *m*O-9-O*m* series exhibit both the N_{TB} and N phases. The N_{TB} phase is extinguished by the emergence of a smectic CA phase with 5O-9-O5, and this increases in stability such that 6O-9-O6 shows a direct SmC_A-I transition. A very similar pattern of behaviour was reported for the nonamethylene-linked phenyl (4-alkoxybenzoate)s for which N and N_{TB} phases were observed up to the hexyloxy homologue for which an anticlinic SmC phase was also seen. For the heptyl homologue the N_{TB} phase was extinguished and this showed the an clinic SmC and N phases, whereas the longer homologues exhibited only the anticlinic SmC phase [47]. The emergence of smectic behaviour for 5O-9-O5 is in accord with the behaviour seen for the *m*O-7-O*m* series and discussed earlier in terms of the relative lengths of the terminal chains and spacer. We have seen, however, that X-ray diffrac on revealed that the ratio of the layer spacer to molecular length in the SmCA phase for 6O-9-O6 is 0.52 and implies an intercalated arrangement of the molecules in which there is a random mixing of the terminal chains and spacers. This is unusual behaviour for symmetric dimers [72]; for example, the *m*.OnO.*m* series only showed monolayer phases [61]. This suggests that the more bent shape associated with the methylene-linked nonyl spacer is assisting in the formation of the intercalated anti-

clinic structure. As discussed already, the texture exhibited by 6O-9-O6 strongly suggests that this is the anticlinic smectic C phase in which the tilt direction alternates on passing from one layer to another. Such an arrangement requires a correlation of the mesogenic units and this may be provided by the flexible spacer endowing molecular curvature, and the intercalation of the terminal chains and spacers. The cross-sectional area of the shorter heptyl spacer would be expected to be less than that of the longer nonyl spacer given the smaller number of conformations available to it. This in turn may inhibit the intercalation of the terminal chains because of the greater mismatch in cross-sectional areas of each component of the molecule. The overlap of the terminal chains and spacers for the *m*O9-O*m* series inhibits the rotation of the molecules around their long axes, and this gives the correlated tilt angle found in the anticlinic smectic C phase. By contrast the *m*O-7-O*m* series exhibits the SmA phase.

It is evident in Fig. 9 that the values of both T_{NI} and T_{NTBN} alternate as *m* is increased and in the same sense, with even members showing the higher values. Similar behaviour can be seen for the *m*O-7-O*m* series in Fig. 8. The dependence of T_{NI} on m may be accounted for in terms of the change in average molecular shape on varying the length of the terminal chains [61,73], and specifically, extending the length of these chains increases the anisotropy of the molecule. This effect is more pronounced when a methylene group is added to an odd membered carbon chain because the additional carbon atom lies more or less parallel to the major axis of the molecule. By comparison, a methylene group added to an even-membered carbon chain to give an odd-membered chain, lies at an angle to this axis, and so a relatively smaller increase in the shape anisotropy is observed. The more linear molecules containing even-membered carbon chains are more compatible with the liquid crystal environment and so higher values of T_{NI} are observed. It appears counterintuitive that the alternation in T_{NTBN} is in the same sense as that seen for T_{NI} on varying m given that it widely accepted that a bent molecular structure is the central prerequisite for the observation of the N_{TB} phase. Indeed, such a view is in accord with predictions made using a generalised Maier-Saupe theory that T_{NTBN} is highly sensitive to the bend angle for V-shaped molecules [74]. It may be expected, therefore, that the even members of a series such as the *m*O-9-O*m* series should exhibit the higher values of T_{NI} based on their greater shape anisotropy but conversely the lower values of T_{NTBN} for exactly the same reason. It has emerged as a quite general observation, however, that on increasing the length of a terminal chain that the alternations seen for T_{NI} and T_{NTBN} are in the same sense [49,50]. It has been suggested that the even members of an alkyloxy chain enhance the anisometric shape of the molecule and also maintain the spatial uniformity of the molecular curvature which is thought to be an important consideration in the formation of the N_{TB} phase [30].

We now turn our attention to the three series in which the length of the spacer is constant but their chemical nature differs: *m*O-7-O*m*, *m*O6O-O*m*, and *m*O-O5O-O*m*. The transitional properties of the *m*O-6O-O*m* series are listed in Table 6. All nine members exhibit a conventional nematic phase, and in addition, the first two show a strongly monotropic twist-bend nematic phase. The dependence of the transition temperatures on the length of the terminal chains, *m*, is shown in Fig. 10, and the trends observed for T_{NI} and $T_{N_{TB}N}$ are essentially identical to those seen from the *m*0-7-0*m* series (Fig.8) although smectic phases are not observed for the *m*0-60-0*m* series.

Table 6
The transitional properties of the *m*O-6O-O*m* series.

m	T_{Cr}/°C	$T_{N_{TB}N}$/°C	T_{NI}/°C	$\Delta S_{Cr}/R$	$\Delta S_{NI}/R$
1	144	103[b]	155	15.87	0.34
2	134	107[b]	164	11.99	0.41
3	142		136[a]	16.06	0.17[a]
4	138		140[a]	16.32	0.36[a]
5	129		129[a]	15.88	0.31[a]
6	132		127[a]	16.67	0.06[a]
7	128		123[a]	17.70	0.13[a]
8	126		125[a]	18.91	0.35[a]
9	126		124[b]	22.54	

[a] Denotes values taken on cooling traces of DSC.
[b] Denotes values from POM.

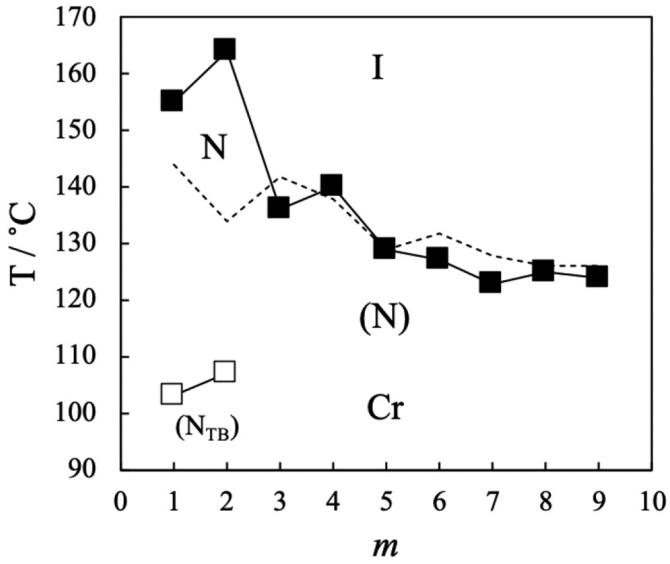

Fig. 10. The dependence of the transition temperatures on the length of the terminal chains, *m*, for the *m*O-6O-O*m* series. The broken line connects the melting points, open squares indicate N-N_{TB} transitions, and filled squares N-I transitions.

Table 7
The transitional properties of the *m*O-O5O-O*m* series.

m	T_{Cr}/°C	T_{NI}/°C	$\Delta S_{Cr}/R$	$\Delta S_{NI}/R$
1	194	186[a]	17.30	0.46[a]
2	186	199	15.51	0.63
3	190	171[a]	18.00	0.51[a]
4	184	176[b]	18.25	
5	177		17.75	
6	173		18.23	
7	170		19.25	
8	168		18.90	
9	165		19.55	

[a] Denotes values taken on cooling traces of DSC.
[b] Denotes values from POM.

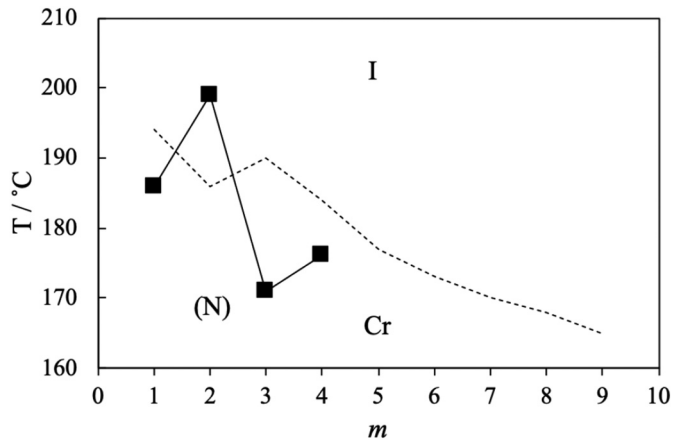

Fig. 11. The dependence of the transition temperatures on the length of the terminal chains, *m*, for the *m*O-O5O-O*m* series. The broken line connects the melting points, and filled squares indicate N-I transitions.

Table 7 lists the transitional properties of the *m*O-O5O-O*m* series, and the dependence of the transition temperatures on *m* shown in Fig. 11. Only the first four members of this series exhibit liquid crystal-line behaviour, a conventional nematic phase. The values of T_{NI} exhibit an odd-even effect as *m* is changed as described for the other series. The absence of liquid crystalline behaviour for the higher members of this series may be attributed to their high melting points.

In considering the comparisons between the transitional properties of the *m*O-7-O*m*, *m*O-6O-O*m*, and *m*O-O5O-O*m* series, we must recall that the shapes of these molecules depend on the differing bond angles between the para axis of the mesogenic unit and the first bond in the spacer. For a methylene link this angle is 113.5° whereas for an ether link it is 126.4°. Thus, a member of the *m*O-O5O-O*m* series is more linear than the corresponding member of the *m*O-7-O*m* series and the curvature of the *m*O-6O-O*m* dimer is intermediate between the two. This dependence of shape on the nature of the spacer was shown for the cyano-terminated dimers in Fig. 7. Fig. 12 compares the melting point of the three series and it is clear the ether-linked *m*O-O5O-O*m* series shows the highest melting points and the methylene-linked *m*O-7-O*m* series the lowest. This may be attributed to the greater linearity of the *m*O-O5O-O*m* series allowing for greater packing efficiency in the crystal phase, as well as enhanced polar interactions arising from the ether links. The melting points of the *m*O-6O-O*m* series fall between those of the other two as may be anticipated.

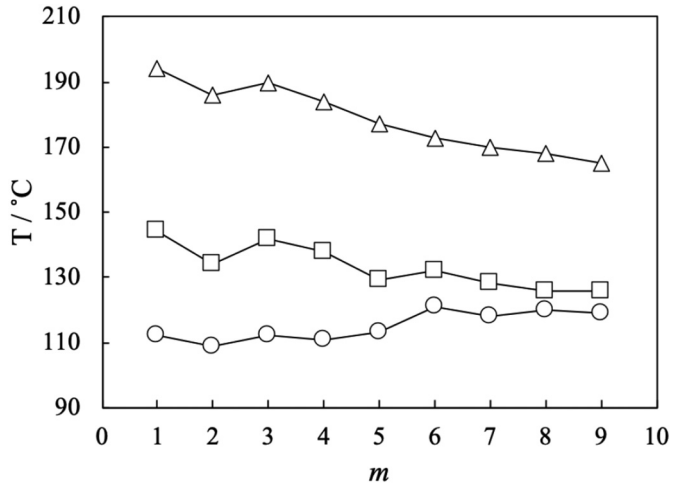

Fig. 12. A comparison of the melting points of the *m*O-7-O*m* (circles), *m*O-6O-O*m* (squares) and *m*O-O5O-O*m* (triangles) series.

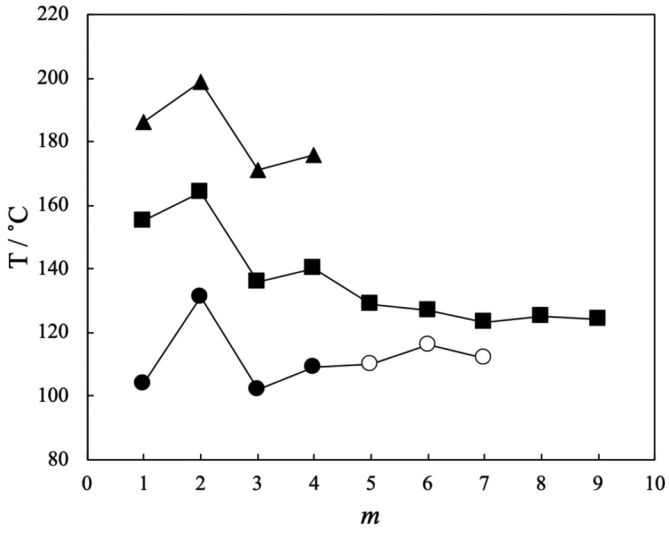

Fig. 13. A comparison of the liquid crystal-isotropic transition temperatures of the *m*O-7-O*m* (circles), *m*O-6O-O*m* (squares) and *m*O-O5O-O*m* (triangles) series. Filled symbols indicate nematic-isotropic transitions, and empty symbols smectic A-isotropic transitions.

The N-I and Sm-I transition temperatures of the three series are compared in Fig. 13 and again the ether-linked dimers show the highest clearing temperatures and the methylene-linked the lowest. The values of T_{NI} for the *m*O-6O-O*m* series fall between those of the other two series. This may be attributed to the relative linearity of these three series. Given the monotropic nature of many of these dimers it is not possible to make a wide-ranging comparison of the values of $\Delta S_{NI}/R$, but where this is possible, those shown by the *m*O-O5O-O*m* are the highest and those for the *m*O-7-O*m* series the lowest. This behaviour is fully in accord with the predictions of the model developed by Luckhurst and co-workers described earlier in which the only difference between the dimers considered are the bond angles between the para axis of the mesogenic unit and the first bond in the spacer [64–66].

Of the 27 dimers in these three series just four exhibit the N_{TB} phase. T_{NTBN} is 16 °C higher for 1O-6O-O1 than for 1O-7-O1, whereas for the second member of these series this is reversed, and T_{NTBN} is 7 °C higher for 2O-7-O2 than for 2O-6O-O2. These observations may be accounted for using the arguments discussed earlier for the cyano-terminated dimers, and specifically, how the shapes of the mesogenic units contribute to the overall molecular shape. As these units become more anisometric, the difficulty associated with packing these nonsymmetric molecules into a bent structure increases, and T_{NTBN} falls relative to T_{NI}. It is interesting to note that the longer members of the *m*O-7-O*m* series ($m \geq 5$) exhibit smectic A-isotropic transitions whereas the corresponding members of the *m*O-6O-O*m* series are exclusively nematic. This observation reinforces the view that the nonsymmetric molecules experience greater difficulty in close packing. Such a view, however, appears at odds with the higher melting points observed for the *m*O-6O-O*m* series, see Fig. 12, and suggests that dipolar interactions may be more important in determining the melting point. Liquid crystalline behaviour is not seen for the corresponding members of the *m*O-O5O-O*m* series, and this is presumably precluded from observation by their high melting points. For the *m*O-5-O*m* series, the longest members (m = 9,1) show an ordered smectic-isotropic transition whereas the corresponding members of the *m*O-O3O-*m* series do not exhibit liquid crystallinity but again have high melting points [53]. We have also seen that the longer members of the *m*O-9-O*m* series show smectic behaviour, see Fig. 9, and it would appear that these bent methylene-linked symmetric dimers have a stronger tendency to exhibit smectic behaviour than the more linear nonsymmetric dimers based on a hexyloxy spacer.

4. Conclusions

The differences between the transitional properties of the dimers reported here may be attributed largely to the difference in their average molecular shapes arising from the different links between the spacer and mesogenic units. The values of T_{NTBN} and T_{NI} for any given dimer appear to depend, at least to some extent, on the shapes of the mesogenic units and how these may be accommodated within the local packing arrangements in the nematic phases. Increasing the terminal chain length in the *m*O-7-O*m* series sees the emergence of a smectic A phase at the expense of the conventional nematic and twist-bend nematic phases. Similar behaviour is observed for the *m*O-9-O*m* series but an anticlinic smectic C phase is observed rather than a smectic A phase. The formation of smectic phases by these series may be attributed to the increased molecular inhomogeneity arising from the terminal chains driving micro-phase separation. The difference in smectic behaviour is attributed to the ability of the terminal chains to intercalate for the dimers having the longer spacer, and this stabilises the alternating tilt found in the anticlinic smectic C phase. A rather general observation has emerged in which T_{NTBN} and T_{NI} alternate in the same sense in a homologous series in which the lengths of terminal chains are varied, and this strongly suggests that the spatial uniformity of the molecular curvature is an important factor in stabilising the N_{TB} phase.

CRediT authorship contribution statement

Ewan Forsyth: Investigation, Writing - original draft, Visualization. Daniel A. Paterson: Investigation. Ewan Cruickshank: Investigation. Grant J. Strachan: Investigation, Visualization. Ewa Gorecka: Investigation, Resources. Rebecca Walker: Investigation, Writing - original draft, Visualization. John M.D. Storey: Resources, Supervision. Corrie T. Imrie: Conceptualization, Resources, Writing - review & editing, Supervision.

Declaration of competing interest

The authors declare that they have no known competing financial interests or personal relationships that could have appeared to influence the work reported in this paper.

Acknowledgements

The work was supported in part by the National Science Centre, Poland under the grant no. 2016/22/A/ST5/00319.

References

[1] M. Cestari, S. Diez-Berart, D.A. Dunmur, A. Ferrarini, M.R. de la Fuente, D.J.B. Jackson, D.O. Lopez, G.R. Luckhurst, M.A. Perez-Jubindo, R.M. Richardson, J. Salud, B.A. Timimi, H. Zimmermann, Phase behavior and properties of the liquid-crystal dimer 1″,7″-bis(4-cyanobiphenyl-4′-yl) heptane: a twist-bend nematic liquid crystal, Phys. Rev. E 84 (2011), 031704.

[2] R.B. Meyer, Structural problems in liquid crystal physics, les houches summer school in theoretical physics, in: R. Balian, G. Weil (Eds.), Molecular Fluids, Gordon and Breach, New York 1976, pp. 273–373.

[3] I. Dozov, On the spontaneous symmetry breaking in the mesophases of achiral banana-shaped molecules, Europhys. Lett. 56 (2001) 247–253.

[4] V. Borshch, Y.K. Kim, J. Xiang, M. Gao, A. Jakli, V.P. Panov, J.K. Vij, C.T. Imrie, M.G. Tamba, G.H. Mehl, O.D. Lavrentovich, Nematic twist-bend phase with nanoscale modulation of molecular orientation, Nat. Commun. 4 (2013) 2635.

[5] R. Walker, D. Pociecha, J.M.D. Storey, E. Gorecka, C.T. Imrie, The chiral twist-bend nematic phase (N*(TB)), Chem. Eur. J. 25 (2019) 13329–13335.

[6] A.A. Dawood, M.C. Grossel, G.R. Luckhurst, R.M. Richardson, B.A. Timimi, N.J. Wells, Y.Z. Yousif, Twist-bend nematics, liquid crystal dimers, structure-property relations, Liq. Cryst. 44 (2017) 106–126.

[7] A.A. Dawood, M.C. Grossel, G.R. Luckhurst, R.M. Richardson, B.A. Timimi, N.J. Wells, Y.Z. Yousif, On the twist-bend nematic phase formed directly from the isotropic phase, Liq. Cryst. 43 (2016) 2–12.

[8] C.T. Archbold, E.J. Davis, R.J. Mandle, S.J. Cowling, J.W. Goodby, Chiral dopants and the twist-bend nematic phase - induction of novel mesomorphic behaviour in an apolar bimesogen, Soft Matter 11 (2015) 7547–7557.

[9] J. Xiang, A. Varanytsia, F. Minkowski, D.A. Paterson, J.M.D. Storey, C.T. Imrie, O.D. Lavrentovich, P. Palffy-Muhoray, Electrically tunable laser based on oblique heliconical cholesteric liquid crystal, Proc. Natl. Acad. Sci. U. S. A. 113 (2016) 12925–12928.

[10] S.M. Salili, J. Xiang, H. Wang, Q. Li, D.A. Paterson, J.M.D. Storey, C.T. Imrie, O.D. Lavrentovich, S.N. Sprunt, J.T. Gleeson, A. Jakli, Magnetically tunable selective reflection of light by heliconical cholesterics, Phys. Rev. E 94 (2016), 042705.

[11] J. Xiang, Y.N. Li, Q. Li, D.A. Paterson, J.M.D. Storey, C.T. Imrie, O.D. Lavrentovich, Electrically tunable selective reflection of light from ultraviolet to visible and infrared by heliconical cholesterics, Adv. Mater. 27 (2015) 3014–3018.

[12] Y. Wang, Z.G. Zheng, H.K. Bisoyi, K.G. Gutierrez-Cuevas, L. Wang, R.S. Zola, Q. Li, Thermally reversible full color selective reflection in a self-organized helical super-structure enabled by a bent-core oligomesogen exhibiting a twist-bend nematic phase, Mater. Horiz. 3 (2016) 442–446.

[13] C.L. Yuan, W.B. Huang, Z.G. Zheng, B.H. Liu, H.K. Bisoyi, Y.N. Li, D. Shen, Y.Q. Lu, Q. Li, Stimulated transformation of soft helix among helicoidal, heliconical, and their in-verse helices, Sci. Adv. 5 (2019), eaax9501.

[14] S. Aya, P. Salamon, D.A. Paterson, J.M.D. Storey, C.T. Imrie, F. Araoka, A. Jakli, A. Buka, Fast-and-giant photorheological effect in a liquid crystal dimer, Adv. Mater. Inter-faces 6 (2019), 1802032.

[15] C.T. Imrie, P.A. Henderson, Liquid crystal dimers and higher oligomers: between monomers and polymers, Chem. Soc. Rev. 36 (2007) 2096–2124.

[16] C.T. Imrie, P.A. Henderson, G.Y. Yeap, Liquid crystal oligomers: going beyond dimers, Liq. Cryst. 36 (2009) 755–777.

[17] A. Lesac, U. Baumeister, I. Dokli, Z. Hamersak, T. Ivsic, D. Kontrec, M. Viskic, A. Knezevic, R.J. Mandle, Geometric aspects influencing N-N-TB transition - implication of intramolecular torsion, Liq. Cryst. 45 (2018) 1101–1110.

[18] D.A. Paterson, J.P. Abberley, W.T. Harrison, J.M. Storey, C.T. Imrie, Cyanobiphenyl-based liquid crystal dimers and the twist-bend nematic phase, Liq. Cryst. 44 (2017) 127–146.

[19] D.A. Paterson, M. Gao, Y.K. Kim, A. Jamali, K.L. Finley, B. Robles-Hernandez, S. Diez-Berart, J. Salud, M.R. de la Fuente, B.A. Timimi, H. Zimmermann, C. Greco, A. Ferrarini, J.M.D. Storey,D.O.Lopez, O.D. Lavrentovich, G.R. Luckhurst, C.T.Imrie, Understanding the twist-bend nematic phase: the characterisation of 1-(4-cyanobiphenyl-4’-yloxy)-6-(4-cyanobiphenyl-4’-yl)hexane (CB6OCB) and comparison with CB7CB, Soft Matter 12 (2016) 6827–6840.

[20] P.A. Henderson, C.T. Imrie, Methylene-linked liquid crystal dimers and the twist-bend nematic phase, Liq. Cryst. 38 (2011) 1407–1414.

[21] E. Cruickshank, M. Salamonczyk, D. Pociecha, G.J. Strachan, J.M.D. Storey, C. Wang, J. Feng, C.H. Zhu, E. Gorecka, C.T. Imrie, Sulfur-linked cyanobiphenyl-based liquid crystal dimers and the twist-bend nematic phase, Liq. Cryst. 46 (2019) 1595–1609.

[22] R.J. Mandle, J.W. Goodby, Molecular flexibility and bend in semi-rigid liquid crystals: implications for the heliconical nematic ground state, Chem. Eur. J. 25 (2019) 14454–14459.

[23] R.J. Mandle, C.T. Archbold, J.P. Sarju, J.L. Andrews, J.W. Goodby, The dependency of nematic and twist-bend mesophase formation on bend angle, Sci. Rep. 6 (2016), 36682.

[24] Y. Arakawa, K. Komatsu, H. Tsuji, Twist-bend nematic liquid crystals based on thioether linkage, New J. Chem. 43 (2019) 6786–6793.

[25] W.D. Stevenson, H.X. Zou, X.B. Zeng, C. Welch, G. Ungar, G.H. Mehl, Dynamic calorimetry and XRD studies of the nematic and twist-bend nematic phase transitions in a series of dimers with increasing spacer length, Phys. Chem. Chem. Phys. 20 (2018) 25268–25274.

[26] R. Walker, The twist-bend phases: structure-property relationships, chirality and hydrogen-bonding, Liq. Cryst. Today 29 (2020) 2–14.

[27] R.J. Mandle, Designing liquid-crystalline oligomers to exhibit twist-bend modulated nematic phases, Chem. Rec. 18 (2018) 1341–1349.

[28] A. Knezevic, M. Sapunar, A. Buljan, I. Dokli, Z. Hamersak, D. Kontrec, A. Lesac, Fine-tuning the effect of pi-pi interactions on the stability of the N-TB phase, Soft Matter 14 (2018) 8466–8474.

[29] J.P. Abberley, J.M.D. Storey, C.T. Imrie, Structure-property relationships in azobenzene-based twist-bend nematogens, Liq. Cryst. 46 (2019) 2102–2114.

[30] D.A. Paterson, J. Xiang, G. Singh, R. Walker, D.M. Agra-Kooijman, A. Martinez-Felipe, M. Gan, J.M.D. Storey, S. Kumar, O.D. Lavrentovich, C.T. Imrie, Reversible isothermal twist-bend nematic-nematic phase transition driven by the photoisomerization of an azobenzene-based nonsymmetric liquid crystal dinner, J. Am. Chem. Soc. 138 (2016) 5283–5289.

[31] J.P. Abberley, S.M. Jansze, R. Walker, D.A. Paterson, P.A. Henderson, A.T.M. Marcelis, J.M.D. Storey, C.T. Imrie, Structure-property relationships in twist-bend nematogens: the influence of terminal groups, Liq. Cryst. 44 (2017) 68–83.

[32] D.A. Paterson, R. Walker, J.P. Abberley, J. Forestier, W.T.A. Harrison, J.M.D. Storey, D. Pociecha, E. Gorecka, C.T. Imrie, Azobenzene-based liquid crystal dimers and the twist-bend nematic phase, Liq. Cryst. 44 (2017) 2060–2078.

[33] J.P. Abberley, R. Walker, J.M.D. Storey, C.T. Imrie, Molecular structure and the twist-bend nematic phase: the role of terminal chains, Liq. Cryst. 47 (2020) 1232–1245.

[34] R.J. Mandle, J.W. Goodby, A liquid crystalline oligomer exhibiting nematic and twist-bend nematic mesophases, Chemphyschem 17 (2016) 967–970.

[35] R.J. Mandle, J.W. Goodby, A nanohelicoidal nematic liquid crystal formed by a non-linear duplexed hexamer, Angew. Chem. Int. Ed. 57 (2018) 7096–7100.

[36] M.R. Tuchband, D.A. Paterson, M. Salamonczykc, V.A. Norman, A.N. Scarbrough, E. Forsyth, E. Garcia, C. Wang, J.M.D. Storey, D.M. Walba, S. Sprunt, A. Jakli, C.H. Zhu, C. T. Imrie, N.A. Clark, Distinct differences in the nanoscale behaviors of the twist-bend liquid crystal phase of a flexible linear trimer and homologous dimer, Proc. Natl. Acad. Sci. U. S. A. 116 (2019) 10698–10704.

[37] Y. Arakawa, K. Komatsu, S. Inui, H. Tsuji, Thioether-linked liquid crystal dimers and trimers: the twist-bend nematic phase, J. Mol. Struct. (2020) 1199.

[38] Y. Wang, G. Singh, D.M. Agra-Kooijman, M. Gao, H.K. Bisoyi, C.M. Xue, M.R. Fisch, S. Kumar, Q. Li, Room temperature heliconical twist-bend nematic liquid crystal, Crystengcomm 17 (2015) 2778–2782.

[39] D. Chen, M. Nakata, R.F. Shao, M.R. Tuchband, M. Shuai, U. Baumeister, W. Weissflog, D.M. Walba, M.A. Glaser, J.E. Maclennan, N.A. Clark, Twist-bend heliconical chiral nematic liquid crystal phase of an achiral rigid bent-core mesogen, Phys. Rev. E 89 (2014), 022506.

[40] S.P. Sreenilayam, V.P. Panov, J.K. Vij, G. Shanker, The N-TB phase in an achiral asymmetrical bent-core liquid crystal terminated with symmetric alkyl chains, Liq. Cryst. 44 (2017) 244–253.

[41] R. Walker, D. Pociecha, A. Martinez-Felipe, J.M.D. Storey, E. Gorecka, C.T. Imrie, Twist-bend nematogenic supramolecular dimers and trimers formed by hydrogen bonding, Crystals 10 (2020) 175.

[42] R. Walker, D. Pociecha, J.P. Abberley, A. Martinez-Felipe, D.A. Paterson, E. Forsyth, G.B. Lawrence, P.A. Henderson, J.M.D. Storey, E. Gorecka, C.T. Imrie, Spontaneous chirality through mixing achiral components: a twist-bend nematic phase driven by hydrogen-bonding between unlike components, Chem. Commun. 54 (2018) 3383–3386.

[43] S.M. Jansze, A. Martinez-Felipe, J.M.D. Storey, A.T.M. Marcelis, C.T. Imrie, A twist-bend nematic phase driven by hydrogen bonding, Angew. Chem. Int. Ed. 54 (2015) 643–646.

[44] Z.B. Lu, P.A. Henderson, B.J.A. Paterson, C.T. Imrie, Liquid crystal dimers and the twist-bend nematic phase. The preparation and characterisation of the alpha, omega-bis(4-cyanobiphenyl-4’-yl) alkanedioates, Liq. Cryst. 41 (2014) 471–483.

[45] R. Walker, D. Pociecha, C.A. Crawford, J.M.D. Storey, E. Gorecka, C.T. Imrie, Hydrogen bonding and the design of twist-bend nematogens, J. Mol. Liq. 303 (2020), 112630.

[46] R. Walker, D. Pociecha, M. Salamonczyk, J.M. Storey, E. Gorecka, C.T. Imrie, Supramo-lecular liquid crystals exhibiting a chiral twist-bend nematic phase, Mater. Adv. (2020)https://doi.org/10.1039/D0MA00302F.

[47] R.J. Mandle, E.J. Davis, C.T. Archbold, C.C.A. Voll, J.L. Andrews, S.J. Cowling, J.W. Goodby, Apolar bimesogens and the incidence of the twist-bend nematic phase, Chem. Eur. J. 21 (2015) 8158–8167.

[48] T. Ivsic, U. Baumeister, I. Dokli, A. Mikleusevic, A. Lesac, Sensitivity of the N-TB phase formation to the molecular structure of imino-linked dimers, Liq. Cryst. 44 (2017) 93–105.

[49] R. Walker, D. Pociecha, G. Strachan, J.M.D.Storey, E. Gorecka, C.T. Imrie, Molecular curvature, specific intermolecular interactions and the twist-bend nematic phase: the synthesis and characterisation of the 1-(4-cyanobiphenyl-4’-yl)-6-(4-alkylanilinebenzylidene-4’-oxy)hexanes (CB6O.m), Soft Matter 15 (2019) 3188–3197.

[50] D.A. Paterson, C.A. Crawford, D.Pociecha, R.Walker, J.M.D.Storey, E. Gorecka, C. T. Imrie, The role of a terminal chain in promoting the twist-bend nematic phase: the synthesis and characterisation of the 1-(4-cyanobiphenyl-4’-yl)-6-(4-alkyloxyanilinebenzylidene-4’-oxy)hexanes, Liq. Cryst. 45 (2018) 2341–2351.

[51] J.P. Abberley, R. Killah, R. Walker, J.M.D. Storey, C.T. Imrie, M. Salamonczyk, C.H. Zhu, E. Gorecka, D. Pociecha, Heliconical smectic phases formed by achiral molecules, Nat. Commun. 9 (2018) 228.

[52] M. Salamonczyk, N. Vaupotic, D. Pociecha, R. Walker, J.M.D. Storey, C.T. Imrie, C. Wang, C.H. Zhu, E. Gorecka, Multi-level chirality in liquid crystals formed by achiral molecules, Nat. Commun. 10 (2019) 1922.

[53] P.A. Henderson, J.M. Seddon, C.T. Imrie, Methylene- and ether-linked liquid crystal dimers II. Effects of mesogenic linking unit and terminal chain length, Liq. Cryst. 32 (2005) 1499–1513.

[54] P.A. Henderson, R.T. Inkster, J.M. Seddon, C.T. Imrie, Highly non-linear liquid crystal tetramers, J. Mater. Chem. 11 (2001) 2722–2731.

[55] P.A. Henderson, O. Niemeyer, C.T. Imrie, Methylene-linked liquid crystal dimers, Liq. Cryst. 28 (2001) 463–472.

[56] M.J. Frisch, et al., Gaussian 09 (Revision B.01), Gaussian Inc., Wallingford CT, 2010.

[57] M. Tarini, P. Cignoni, C. Montani, Ambient occlusion and edge cueing for enhancing real time molecular visualization, IEEE Trans. Vis. Comput. Graph. 12 (2006) 1237–1244.

[58] J.W. Emsley, G. De Luca, A. Lesage, D. Merlet, G. Pileio, The structure and conformation of a mesogenic compound between almost zero and almost complete orientational order, Liq. Cryst. 34 (2007) 1071–1093.

[59] G.S. Attard, S. Garnett, C.G. Hickman, C.T. Imrie, L. Taylor, Asymmetric dimeric liquid-crystals with charge-transfer groups, Liq. Cryst. 7 (1990) 495–508.

[60] T. Donaldson, H. Staesche, Z.B. Lu, P.A. Henderson, M.F. Achard, C.T. Imrie, Symmetric and non-symmetric chiral liquid crystal dimers, Liq. Cryst. 37 (2010) 1097–1110.

[61] R.W. Date, C.T. Imrie, G.R. Luckhurst, J.M. Seddon, Smectogenic dimeric liquid-crystals - the preparation and properties of the alpha,omega-bis(4-normal-alkylanilinebenzylidine-4'-oxy)alkanes, Liq. Cryst. 12 (1992) 203–238.

[62] R.J. Mandle, E.J. Davis, C.C.A. Voll, C.T. Archbold, J.W. Goodby, S.J. Cowling, The relationship between molecular structure and the incidence of the N-TB phase, Liq. Cryst. 42 (2015) 688–703.

[63] C.T. Archbold, J.L. Andrews, R.J. Mandle, S.J. Cowling, J.W. Goodby, Effect of the linking unit on the twist-bend nematic phase in liquid crystal dimers: a comparative study of two homologous series of methylene- and ether-linked dimers, Liq. Cryst. 44 (2017) 84–92.

[64] A.P.J. Emerson, G.R. Luckhurst, On the relative propensities of ether and methylene linkages for liquid-crystal formation in calamitics, Liq. Cryst. 10 (1991) 861–868.

[65] A. Ferrarini, G.R. Luckhurst, P.L. Nordio, S.J. Roskilly, Prediction of the transitional properties of liquid-crystal dimers - a molecular-field calculation based on the sur-face tensor parametrization, J. Chem. Phys. 100 (1994) 1460–1469.

[66] A. Ferrarini, G.R. Luckhurst, P.L. Nordio, S.J. Roskilly, Understanding the dependence of the transitional properties of liquid crystal dimers on their molecular geometry, Liq. Cryst. 21 (1996) 373–382.

[67] R.J. Mandle, M.P. Stevens, J.W. Goodby, Developments in liquid-crystalline dimers and oligomers, Liq. Cryst. 44 (2017) 2046–2059.

[68] M. Cestari, E. Frezza, A. Ferrarini, G.R. Luckhurst, Crucial role of molecular curvature for the bend elastic and flexoelectric properties of liquid crystals: mesogenic dimers as a case study, J. Mater. Chem. 21 (2011) 12303–12308.

[69] A.E. Blatch, G.R. Luckhurst, The liquid crystal properties of symmetric and non-symmetric dimers based on the azobenzene mesogenic group, Liq. Cryst. 27 (2000) 775–787.

[70] G.S. Attard, R.W. Date, C.T. Imrie, G.R. Luckhurst, S.J. Roskilly, J.M. Seddon, L. Taylor, Nonsymmetrical dimeric liquid-crystals - the preparation and properties of the alpha-(4-cyanobiphenyl-4'-yloxy)-omega-(4-n-alkylanilinebenzylidene-4'-o xy)al-kanes, Liq. Cryst. 16 (1994) 529–581.

[71] C.T. Imrie, Non-symmetric liquid crystal dimers: how to make molecules intercalate, Liq. Cryst. 33 (2006) 1449–1454.

[72] C.T. Imrie, P.A. Henderson, Liquid crystal dimers and oligomers, Curr. Opin. Colloid Interface Sci. 7 (2002) 298–311.

[73] C.T. Imrie, L. Taylor, The preparation and properties of low molar mass liquid-crystals possessing lateral alkyl chains, Liq. Cryst. 6 (1989) 1–10.

[74] C. Greco, G.R. Luckhurst, A. Ferrarini, Molecular geometry, twist-bend nematic phase and unconventional elasticity: a generalised Maier-Saupe theory, Soft Matter 10 (2014) 9318–9323.

Supplementary Information

Liquid crystal dimers and the twist-bend nematic phase: on the role of spacers and terminal alkyl chains

Ewan Forsyth, Daniel A Paterson[1], Ewan Cruickshank, Grant J Strachan, Ewa Gorecka[a], Rebecca Walker, John MD Storey, and Corrie T Imrie[*]

Department of Chemistry, School of Natural and Computing Sciences, University of Aberdeen, Meston Building, Aberdeen AB24 3UE, UK

[a]*Department of Chemistry, University of Warsaw, ul. Zwirki i Wigury 101, 02-089 Warsaw, Poland.*

*Author for correspondence; email c.t.imrie@abdn.ac.uk

[1]Present address: School of Physics and Astronomy, and School of Chemistry, University of Leeds, Leeds, LS2 9JT, UK

Section 1: Reagents, General Techniques, and Instrumentation

1.1 Reagents

All of the reagents and solvents used were commercially available at time of purchase and obtained from various suppliers and used without further purification unless otherwise stated.

Suppliers: ACROS Organics, Alfa Aesar, Fluorochem, Sigma Aldrich, TCI Chemicals.

1.2 General Techniques

Reactions were monitored by thin layer chromatography (TLC), unless otherwise stated, using aluminium-backed sheets with a coating of Merck Kieselgel 60 F254 silica, and were purchased from Merck KGaA.

Compound separation by column chromatography was carried out using silica gel grade 60 Å 40-63 μm particle size, purchased from Fluorochem. The column length and diameter were chosen based on crude mass and previous column chromatography separations where possible. Purification by column chromatography is denoted by '(SiO_2, Solvent system)' along with the solvent system used.

1.3 Structure Analysis

^{1}H and ^{13}C NMR spectra were recorded on either a Bruker Avance III HD 400 NMR, or a 300 MHz Bruker Ultrashield NMR spectrometer. Infrared spectra were recorded on a Thermo Scientific Nicolet IR100 FTIR spectrometer with an ATR diamond cell.

1.4 Purity Analysis

The purities of the final products where possible were verified using either C, H, N microanalysis. C, H, N microanalysis was performed at either; Sheffield Analytical and Scientific Services Elemental Microanalysis Service at the University of Sheffield; the Analysis Services Elemental Microanalysis Service at OEA labs; Centre for Chemical and Material Analysis at the University of Birmingham. QTof mass spectrometry was performed at the University of Aberdeen on a Waters XEVO G2 Q-Tof, S/N YCA247K. Calibration: Sodium formate. Lock mass: leucine enkephalin, $C_{28}H_{37}N_5O_7$ $[M^+H]^+$: 556.2771.

Section 2: Synthetic Procedures

2.1 1,5-Bis(4-acetamidophenyl-4'-oxy)pentane (**I-1**)

The methodology for the synthesis of **I-1** was previously described by Henderson *et al.* [1]

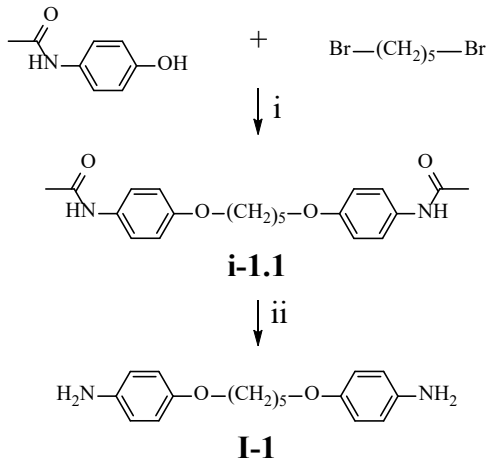

i) K_2CO_3, acetone, 56 °C
ii) NaOH (aq), EtOH, 78 °C

Scheme 1: Synthetic route to form 1,5-bis(4-acetamidophenyl-4'-oxy)pentane (**I-1**)

i-1.1 1,5-bis(4-acetamidophenyl-4'-oxy)pentane

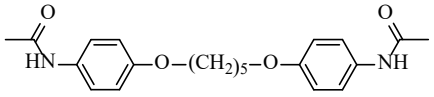

To a stirring solution of acetaminophen (10.000 g, 0.066 mol) and 1,5-dibromopentane (6.760 g, 4.0 mL, 0.029 mol) in acetone (200 mL) was added potassium carbonate (12.024 g, 0.087 mol). The reaction mixture was stirred at 56 °C until TLC indicated near complete consumption of acetaminophen R_f 0.43 (EtOAc) after 24 hours. The reaction was cooled to room temperature, poured into H_2O (500 mL) and the resultant precipitate was collected by filtration. The crude product was purified by recrystallisation from EtOH (400 mL) to give the title compound as a white powder.

Yield: 6.408 g, 59 %

m.p. = 210–212 ˚C

R_f (EtOAc) 0.17

^{1}H NMR (300 MHz, DMSO-d_6) δ 9.80 (s, 2H, 2 × Ac-NH), 7.45 (d, J = 9.0 Hz, 4H, 4 × Ar-H), 6.84 (d, J = 9.0 Hz, 4H, 4 × Ar-H), 3.93 (t, J = 6.4 Hz, 4H, 2 × CH_2-O), 1.99 (s, 6H, 2 × CH_3-CO), 1.75 (quin, J = 6.8 Hz, 4H, 2 × O-CH_2-CH_2), 1.63 – 1.48 (m, 2H, O-CH_2-CH_2-CH_2).

^{13}C NMR (75 MHz, DMSO-d_6) δ 167.64 (2 × CO-NH), 154.37 (2 × Ar-O), 132.45 (2 × Ar-NHAc), 120.46 (4 × Ar-H), 114.34 (4 × Ar-H), 67.46 (2 × CH_2-O), 28.47 (2 × O-CH_2-CH_2), 23.76 (2 × CH_3-CO), 22.24 (O-CH_2-CH_2-CH_2).

IR ν (cm^{-1}): 3292 (CONH); 2949, 2867 (CH_2); 1657 (CO); 1596, 1511 (Ar); 824 (*p*-disub. Ar).

I-1 1,5-Bis(4-aminophenyl-4'-oxy)pentane

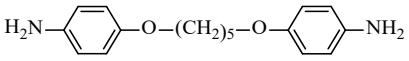

To a stirring solution of **i-1.1** (3.000 g, 8.098 mmol) in EtOH (100 mL) at 78 °C was added in one portion an aqueous solution of NaOH (16.197 g, 0.405 mol) in H_2O (25 mL). The reaction was monitored by TLC until the complete consumption of **4.7** after 1 hour and the consumption of the mono-hydrolysed product (not isolated, R_f (EtOAc) 0.50) after 3 hours. The reaction mixture was cooled, the solvent was removed *in vacuo* to half volume then poured into H_2O (300 mL). The resultant solid was collected by filteration to give the title compound as a tan solid. The product was used without further purification.

Yield: 1.229 g, 53 %

m.p. = 82–84 ˚C

R_f (EtOAc) 0.45

^{1}H NMR (400 MHz, DMSO-d_6) δ 6.63 (d, J = 8.7 Hz, 4H, 4 × Ar-H), 6.49 (d, J = 8.8 Hz, 4H, 4 × Ar-H), 4.56 (s, 4H, 2 × NH_2), 3.81 (t, J = 6.4 Hz, 4H, 2 × CH_2-O), 1.68 (quin, J = 6.8 Hz, 4H, O-CH_2-CH_2), 1.57 – 1.43 (m, 2H O- CH_2-CH_2-CH_2).

^{13}C NMR (101 MHz, DMSO-d_6) δ 150.01 (2 × Ar-O), 142.30 (2 × Ar-NH_2), 115.38 (4 × Ar-H), 114.96 (4 × Ar-H), 67.90 (2 × CH_2-O), 28.74 (2 × O-CH_2-CH_2), 22.38 (CH_2).

IR ν (cm^{-1}): 3433, 3353 (Ar. NH_2); 2950, 2868 (CH_2); 1225 (Ar. C-N); 824 (*p*-disub. Ar)

2.2 1-(4-Aminophenoxy)-6-(4-aminophenyl)hexane (**I-2**)

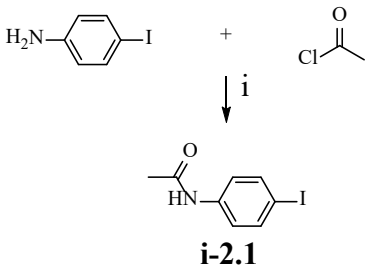

i-2.1

i) Et_3N, EtOAc

Scheme 2: Synthetic route to form 4-iodoacetanilide (**i-2.1**)

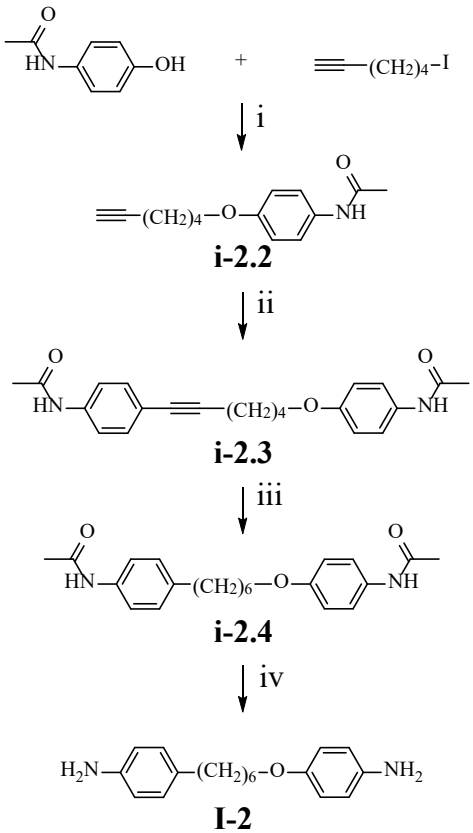

i) K_2CO_3, acetone, 56 ^oC
ii) **i-2.1**, $[Pd(PPh_3)_2Cl_2]$, CuI, iPr_2NH, THF (g), EtOH:EtOAc (1:2) (V/V)
iii) PtO_2, H_2
iv) $NaOH_{(aq)}$, EtOH, 78 ^oC

Scheme 3: Synthetic route to form 1-(4-aminophenoxy)-6-(4-aminophenyl)hexane (**I-2**)

i-2.1 4-Iodoacetanilide

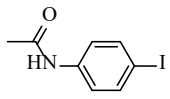

To a cooled stirring solution of 4-iodoaniline (25.000 g, 0.114 mol) in EtOAc (150 mL) was added triethylamine (14.520 g, 20 mL, 0.143 mol) in one portion followed by the dropwise addition of a solution of acetyl chloride (16.500 g, 15 mL, 0.210 mol) in EtOAc (50 mL) over 30 minutes. After the complete addition of acetyl chloride the reaction was heated to room temperature and monitored by TLC until the complete consumption of 4-iodoaniline R_f 0.72 (EtOAc-light petroleum 40/60, 1:1) and the formation of product after 23 hours. Distilled water (200 mL) and EtOAc (50 mL) was added to the reaction mixture and stirred for 15 minutes. The aqueous and organic phases were then separated. The aqueous phase was extracted with EtOAc (100 mL × 2). The organic fractions were combined, washed sequentially with distilled water (50 mL × 2) and brine (50 mL × 2), then dried ($MgSO_4$). The solvent was removed *in vacuo* to give a grey solid. The crude product was purified by the addition of EtOAc (20 mL) and filtered to give the title compound as white crystals.

Yield: 21.716 g, 73%

m.p. = 181–183 ˚C

R_f (EtOAc-light petroleum 40/60, 1:1) 0.59

^{1}H NMR (400 MHz, DMSO-d_6) δ 10.02 (s, 1H, Ac-NH), 7.61 (d, J = 8.8 Hz, 2H, 2 × Ar-H), 7.41 (d, J = 8.8 Hz, 2H 2 × Ar-H), 2.03 (s, 3H, CH_3-CO).

^{13}C NMR (101 MHz, DMSO-d_6) δ 168.45 (CO-NH), 139.13 (Ar-NHAc), 137.28 (2 × Ar-H), 121.13 (2 × Ar-H), 86.29 (Ar-I), 24.05 (CH_3-CO).

IR ν (cm^{-1}): 3288 (CONH); 1666 (CO); 815 (*p*-disub. Ar).

i-2.2 4-(5-Hexyn-1-yloxy)acetanilide

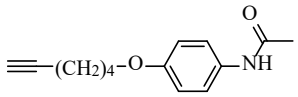

To a stirring solution of acetaminophen (6.557 g, 0.043 mol) and 6-iodohex-1-yne (9.500 g, 6.2 mL, 0.046 mol) in acetone (100 mL), was added potassium carbonate (12.715 g, 0.092 mol). The reaction mixture was stirred at 56 °C until TLC indicated the complete consumption of acetaminophen R_f 0.43 (EtOAc) after 48 hours. The reaction mixture was cooled to room temperature, filtered and the precipitate was washed with EtOAc (200 mL). The solvent was removed from the combined organic phases *in vacuo* to give a crude solid product. The crude product was purified (SiO_2, EtOAc) to give the title compound as a light-brown powder.

Yield: 2.841 g, 27 %

m.p. = 103–105 ˚C

R_f (EtOAc) 0.71

^{1}H NMR (400 MHz, DMSO-d_6) δ 9.75 (s, 1H, Ac-NH), 7.45 (d, J = 9.0 Hz, 2H, 2 × Ar-H), 6.85 (d, J = 9.0 Hz, 2H, 2 × Ar-H), 3.92 (t, J = 6.4 Hz, 2H, O-CH_2), 2.78 (t, J = 2.7 Hz, 1H, C≡CH), 2.22 (td, J = 7.1, 2.6 Hz, 2H, HC≡C-CH_2-CH_2), 1.99 (s, 3H, CH_3-CO), 1.77 (quin, J = 6.6 Hz, 2H, CH_2-CH_2-CH_2), 1.58 (quin, J = 7.1 Hz, 2H, CH_2-CH_2-CH_2).

^{13}C NMR (75 MHz, DMSO-d_6) δ 167.67 (CO-NH), 154.33 (Ar-O), 132.48 (Ar-NHAc), 120.46 (2 × Ar-H), 114.36 (2 × Ar-H), 84.31 (C≡C-H), 71.41 (C≡C-H), 66.99 (CH_2-O), 27.84 (CH_2), 24.66 (CH_2), 23.81 (CH_3-CO), 17.45 (CH_2).

IR ν (cm^{-1}): 3247 (COHN); 2936, 2870 (CH_2); 1653 (CO); 1604, 1509 (Ar), 836 (*p*-disub. Ar).

i-2.3 1-(4-Acetamidophenoxy)-6-(4-acetamidophenyl)hex-5-yne

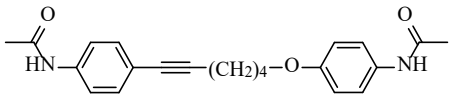

To a solution of **i-2.1** (3.352 g, 0.013 mol) and **i-2.2** (2.700 g, 0.012 mol) in anhydrous THF (50 mL) was added diisopropylamine (20 mL). The reaction mixture was stirred and sparged with argon (g) for 2 hours. To the reaction mixture was added bis(triphenylphosphine)palladium(II) dichloride (0.082 g, 0.117 mmol) followed by copper (I) iodide (0.022 g, 0.117 mmol). The reaction headspace was evacuated and replaced with argon (g) (repeat × 2), The reaction was monitored by TLC until the complete consumption of **i-2.2** after 24 hours. The reaction mixture was filtered through a pad of celite, which was washed with THF (100 mL), followed by EtOAc (100 mL). The organic solvent mixture was removed *in vacuo* and the resultant solid was dissolved in EtOAc (400 mL) which was washed with H_2O (4 × 50 mL) and dried ($MgSO_4$). The solvent was removed *in vacuo*, and the crude product was purified (SiO2, EtOAc) to give the title compound as an off-white powder.

Yield: 3.297 g, 78 %

m.p. = 160–164 ˚C

R_f (EtOAc) 0.30

^{1}H NMR (300 MHz, DMSO-d_6) δ 10.04 (s, 1H, Ac-NH, O side), 9.76 (s, 1H, Ac-NH, C≡C side), 7.54 (d, J = 8.7 Hz, 2H, 2 × Ar-H, C≡C side), 7.45 (d, J = 9.1 Hz, 2H, 2 × Ar-H, O side), 7.29 (d, J = 8.6 Hz, 2H, 2 × Ar-H, C≡C side), 6.86 (d, J = 9.0 Hz, 2H, 2 × Ar-H, O side), 3.96 (t, J = 6.3 Hz, 2H, CH_2-O), 2.45 (t, J = 6.9 Hz, 2H, CH_2-C≡C), 2.04 (s, 3H, CH_3-CO, C≡C side), 1.99 (s, 3H, CH_3-CO, O side), 1.90 – 1.75 (m, 2H, CH_2), 1.75 – 1.58 (m, 2H, CH_2).

^{13}C NMR (75 MHz, DMSO-d_6) δ 168.40 (CO-NH), 167.68 (CO-NH), 154.33 (Ar-O), 138.96 (Ar-NHAc, C≡C side), 132.50 (Ar-NHAc, O side), 131.76 (2 × Ar-H), 120.46 (2 × Ar-H), 118.73 (2 × Ar-H), 117.43 (Ar-C≡C), 114.39 (2 × Ar-H), 89.23 (C≡C-H), 80.77 (C≡C-H), 67.05 (CH_2-O), 28.00 (CH_2), 24.95(CH_2), 24.06 (CH_3-CO), 23.82 (CH_3-CO), 18.42 (CH_2).

IR ν (cm^{-1}): 3292 (COHN); 2934, 2868 (CH_2); 1659 (CO); 1585, 1509 (Ar), 819 (*p*-disub. Ar).

i-2.4 1-(4-Acetamidophenoxy)-6-(4-acetamidophenyl)hexane

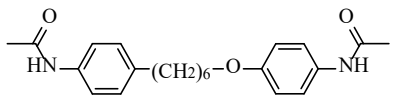

To a stirring solution of **i-2.3** (3.197 g, 8.772 mmol) in EtOH/EtOAc (300 mL, 1:2 EtOH:EtOAc V/V) was added platinum dioxide (0.050 g, 0.220 mmol). The reaction mixture was sparged with H_2 (g) (approx. 5 L) with constant stirring. The reaction headspace was evacuated and replaced with H_2 (g) (repeat × 2) and the reaction progress was monitored by NMR until the consumption of **i-2.3** after 24 hours. The reaction mixture was filtered through a pad of celite, which was washed with EtOAc (200 mL), and then solvent removed *in vacuo*. The crude product was purified (SiO_2, EtOAc) to give the title compound as an off-white powder.

Yield: 1.908g, 59 %

m.p. = 174–180 ˚C

R_f (EtOAc) 0.26

^{1}H NMR (300 MHz, DMSO-d_6) δ 9.82 (s, 1H, Ac-NH, O side), 9.75 (s, 1H, Ac-NH, C≡C side), 7.45 (2 × d overlapping (observed as dd), J = 8.8, 2.4 Hz, 4H, 4 × Ar-H), 7.09 (d, J = 8.4 Hz, 2H, 2 × Ar-H), 6.83 (d, J = 9.0 Hz, 2H, 2 × Ar-H), 3.88 (t, J = 6.4 Hz, 2H, CH_2-O), 2.53 (t (overlapping with DMSO-d_6), 2H, CH_2-Ar), 2.01 (s, 3H CH_3-CO, CH_2 side), 1.99 (s, 3H, CH_3-CO, O side), 1.66 (quin, J = 6.6 Hz, 2H, CH_2), 1.55 (quin, J = 7.5 Hz, 2H, CH_2), 1.49 – 1.23 (m, 4H, 2 × CH_2).

^{13}C NMR (75 MHz, DMSO-d_6) δ 167.97 (CO-NH), 167.65 (CO-NH), 154.39 (Ar-O), 137.01 (Ar), 136.81 (Ar), 132.40 (Ar-NHAc, O side), 128.35 (2 × Ar-H), 120.47 (2 × Ar-H), 118.99 (2 × Ar-H), 114.33 (2 × Ar-H), 67.46 (CH_2-O), 34.47 (CH_2), 30.98 (CH_2), 28.67 (CH_2), 28.34 (CH_2), 25.35 (CH_2), 23.92 (CH_3-CO), 23.79 (CH_3-CO).

IR ν (cm^{-1}): 3294 (COHN); 2926, 2858 (CH_2); 1656 (CO); 1595, 1509 (Ar), 819 (*p*-disub. Ar).

i-2.5 1-(4-Aminophenoxy)-6-(4-aminophenyl)hexane

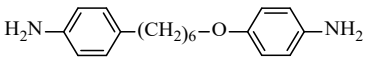

Synthesis procedure follows that described for **I-1** 1,5-bis(4-aminophenyl-4'-oxy)pentane

Quantities used: **i-2.4** (1.800 g, 4.885 mmol); EtOH (150 mL); NaOH (5.862 g, 0.147 mol) in H_2O (35 mL).

TLC indicated the complete consumption of **i-2.4** after 3 hours and the mono-hydrolysed product (not isolated, R_f (EtOAc) 0.42) after 20 hours.

The crude product was purified (SiO_2, EtOAc-light petroleum 40/60, 7:3), followed by recrystallisation from EtOH/H_2O (1:1 (V/V), 60 mL) to give to give the title compound as an off-white powder.

Yield: 1.009 g, 73 %

m.p. = 39–41 ˚C

R_f (EtOAc-light petroleum 40/60, 7:3) 0.30

^{1}H NMR (400 MHz, DMSO-d_6) δ 6.82 (d, J = 8.0 Hz, 2H), 6.61 (d, J = 8.8 Hz, 2H), 6.51 – 6.44 (m, 3H), 4.77 (s, 2H, Ar-$\underline{NH_2}$ methylene side), 4.56 (s, 2H, Ar-$\underline{NH_2}$ ether side), 3.78 (t, J = 6.5 Hz, 2H, O-$\underline{CH_2}$), 2.38 (t, J = 7.6 Hz, 2H, Ar-$\underline{CH_2}$), 1.61 (quin, J = 6.8 Hz, 2H, CH_2), 1.49 (quin, J = 7.5 Hz, 2H, CH_2), 1.38 (quin, J = 7.2 Hz, 2H, CH_2), 1.34 – 1.23 (m, 2H, CH_2).

^{13}C NMR (75 MHz, DMSO-d_6) δ 149.97 ($\underline{Ar}$-O), 146.33 ($\underline{Ar}$-NH_2 methylene side), 142.30 ($\underline{Ar}$-NH_2 ether side), 129.25 ($\underline{Ar}$-CH_2), 128.62 (2 × Ar-H), 115.31 (2 × Ar-H), 114.93 (2 × Ar-H), 113.96 (2 × Ar-H), 67.83 ($\underline{CH_2}$-O), 34.36 (CH_2), 31.48 (CH_2), 28.95 (CH_2), 28.45 (CH_2), 25.49 (CH_2).

IR ν (cm^{-1}): 3368, 3289 (Ar. NH_2); 2928, 2850 (CH_2); 1614, 1508 (Ar) 1238 (Ar. C-N); 805 (*p*-disub. Ar).

2.3 1,7-Bis(4-phenylacetamide-4'-)heptane (**I-3-7**) and
1,9-bis(4-phenylacetamide-4'-)nonane (**I-3-9**).

2.3.1 Method 1

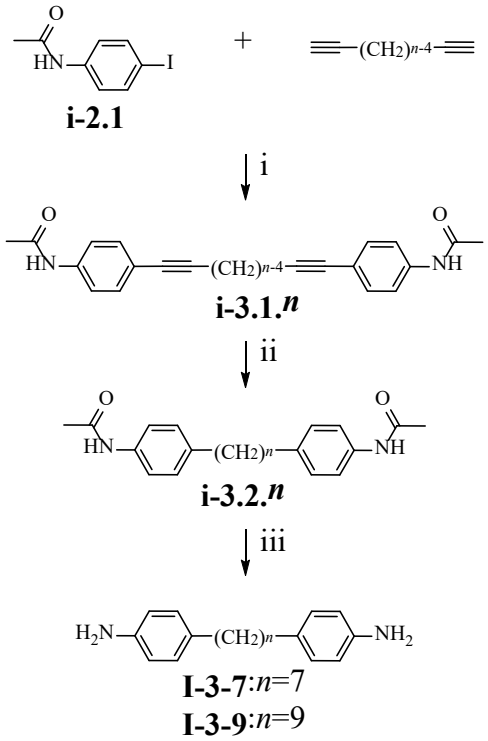

i) $[Pd(PPh_3)_2Cl_2]$, CuI, iPr_2NH, THF (g), EtOH:EtOAc (1:2) (V/V)
ii) PtO_2, H_2
iii) $NaOH_{(aq)}$, EtOH, 78 ^oC

Scheme 4: Synthetic route to form the *a,ω*-bis(4-aminophenyl-4'-)alkanes (**I-3-7** and **I-3-9**) by method 1.

i-3.1.7 1,7-Bis(4-phenylacetamide-4'-)hepta-1,6-diyn

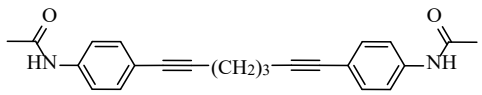

Synthesis procedure follows that described for **i-2.3** 1-(4-acetamidophenoxy)-6-(4-acetamidophenyl)hex-5-yne.

Quantities used: **i-2.1** (10.000 g, 0.038 mol); 1,6-heptadiyne (1.771 g, 2.2 mL, 0.019 mol); THF (80 mL), diisopropylamine (20 mL); bis(triphenylphosphine)palladium(II) dichloride (0.133 g, 0.190 mmol); copper (I) iodide (0.724 g, 0.38 mmol, 2 mol%).

TLC indicated the complete consumption of **i-2.1** after 48 hours.

The crude product was purified (SiO_2, EtOAc) to give the title compound as an off-white powder.

Yield: 4.568 g, 67%

m.p. = 195–200 ˚C

R_f (EtOAc) 0.29

^{1}H NMR (400 MHz, DMSO-d_6) δ 10.03 (s, 2H, 2 × Ac-NH), 7.55 (d, J = 8.8 Hz, 4H, 4 × Ar-H), 7.32 (d, J = 8.7 Hz, 4H, 4 × Ar-H), 2.54 (t, J = 7.1 Hz, 4H, 2 × C≡C-CH_2), 2.04 (s, 6H, 2 × CH_3-CO), 1.79 (quin, J = 7.1 Hz, 2H, CH_2-CH_2-CH_2).

^{13}C NMR (101 MHz, DMSO-d_6) δ 168.41 (2 × CO-NH), 139.03 (2 × Ar-NHAc), 131.82 (4 × Ar-H), 118.72 (4 × Ar-H), 117.30 (2 × Ar-C≡C), 88.57 (2 × Ar-C≡C), 81.03 (2 × Ar-C≡C), 27.68 (CH_2-CH_2-CH_2), 24.06 (2 × CH_3-CO), 17.99 (2 × C≡C-CH_2).

IR ν (cm^{-1}): 3301 (COHN); 1667 (CO); 1599, 1508 (Ar), 836 (*p*-disub. Ar).

i-3.1.9 1,9-Bis(4-phenylacetamide-4'-)nona-1,8-diyn

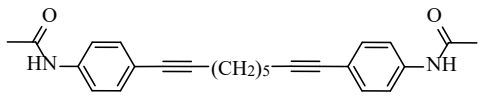

Synthesis procedure follows that described for **i-2.3** 1-(4-acetamidophenoxy)-6-(4-acetamidophenyl)hex-5-yne.

Quantities used: **i-2.1** (5.000 g, 0.019 mol); 1,8-nonadiyne (1.151 g, 1.4 mL, 0.010 mol); THF (70 mL), diisopropylamine (40 mL); bis(triphenylphosphine)palladium(II) dichloride (0.134 g, 0.192 mmol); copper (I) iodide (0.019 g, 0.100 mmol).

TLC indicated the complete consumption of **i-2.1** after 24 hours.

The crude product was purified (SiO_2, EtOAc) to give the title compound as an off-white powder.

Yield: 2.453 g, 67 %

m.p. = 158–163 ˚C

R_f (EtOAc) 0.21

^{1}H NMR (400 MHz, DMSO-d_6) δ 10.01 (s, 2H, 2 × Ac-NH), 7.53 (d, J = 8.4 Hz, 4H, 4 × Ar-H), 7.28 (d, J = 8.6 Hz, 4H, 4 × Ar-H), 2.47 – 2.38 (t (observed as m), 4H, 2 × C≡C-CH_2), 2.04 (s, 6H, 2 × CH_3-CO), 1.64 – 1.52 (m, 6H, 3 × CH_2).

^{13}C NMR (101 MHz, DMSO-d_6) δ 168.37 (2 × CO-NH), 138.90 (2 × Ar-NHAc), 131.70 (4 × Ar-H), 118.74 (4 × Ar-H), 117.51 (2 × Ar-C≡C), 89.40 (2 × Ar-C≡C), 80.62 (2 × Ar-C≡C), 27.77 (2 × C≡C-CH_2-CH_2), 24.04 (2 × CH_3-CO), 18.58 (2 × C≡C-CH_2).

IR ν (cm^{-1}): 3312 (COHN); 2929, 2857 (CH_2); 1654 (CO); 1588, 1526 (Ar), 835 (*p*-disub. Ar).

i-3.2.7 1,7-bis(4-phenylacetamide-4'-)heptane

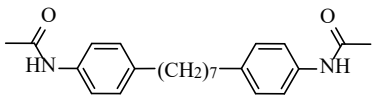

Synthesis procedure follows that described for **i-2.4** 1-(4-acetamidophenoxy)-6-(4-acetamidophenyl)hexane

Quantities used: **i-3.1.7** (4.400 g, 0.012 mol); platinum dioxide (0.100 g, 0.044 mmol); EtOAc/EtOH (400 mL, 2:1 EtOAc:EtOH V/V);. H_2 (g) (approx. 10 L).

Reaction was monitored by NMR until the complete consumption of **i-3.1.7** after 48 hours.

The crude product was purified by recrystallisation from toluene (150 mL) to give the title compound as a white powder.

Yield: 2.763 g, 61 %

m.p. = 185–189 ˚C

R_f (EtOAc) 0.30

^{1}H NMR (400 MHz, DMSO-d_6) δ 9.81 (s, 2H, 2 × Ac-NH), 7.45 (d, J = 8.4 Hz, 4H, 4 × Ar-H), 7.07 (d, J = 8.4 Hz, 4H, 4 × Ar-H), 2.47 (t, J = 7.9 Hz, 4H, 2 × Ar-CH_2), 2.01 (s, 6H, 2 × CH_3-CO), 1.50 (quin, J = 7.4 Hz, 4H, 2 × Ar-CH_2-CH_2), 1.34 – 1.17 (m, 6H, 3 × CH_2).

^{13}C NMR (101 MHz, DMSO-d_6) δ 167.96 (2 × CO-NH), 136.99 (2 × Ar-X), 136.84 (2 × Ar-X), 128.33 (4 × Ar-H, CH_2 side), 118.98 (4 × Ar-H, NHAc side), 34.50 (2 × CH_2), 30.98 (2 × CH_2), 28.63 (CH_2), 28.52 (2 × CH_2), 23.92 (2 × CH_3-CO).

IR ν (cm^{-1}): 3293 (COHN); 2918, 2849 (CH_2); 1660 (CO); 1596, 1532 (Ar), 837 (*p*-disub. Ar).

i-3.2.9 1,9-Bis(4-phenylacetamide-4'-)nonane

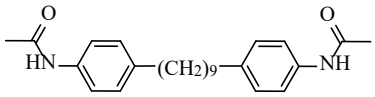

Synthesis procedure follows that described for **i-2.4** 1-(4-acetamidophenoxy)-6-(4-acetamidophenyl)hexane

Quantities used: **i-3.1.9** (2.300 g, 5.951 mmol); platinum dioxide (0.100 g, 0.044 mmol); EtOAc/EtOH (300 mL, 2:1 EtOAc:EtOH V/V);. H_2 (g) (approx. 10 L).

Reaction was monitored by NMR until the complete consumption of **i-3.1.9** after 48 hours.

The crude product was purified (SiO_2, EtOAc) to give the title compound as a white powder.

m.p. = 160–165 ˚C

Yield: 2.134 g, 91 %

R_f (EtOAc) 0.40

^{1}H NMR (400 MHz, DMSO-d_6) δ 9.81 (s, 2H, 2 × Ac-NH), 7.45 (d, J = 8.2 Hz, 4H, 4 × Ar-H), 7.07 (d, J = 8.2 Hz, 4H, 4 × Ar-H), 2.50 – 2.42 (2 × t (overlapping with DMSO-d_6, observed as m), 4H, 2 × Ar-CH_2), 2.01 (s, 6H, 2 × CH_3-CO), 1.50 (quin, J = 7.3 Hz, 4H, 2 × Ar-CH_2-CH_2), 1.31 – 1.17 (m, 10H, 5 × CH_2).

^{13}C NMR (101 MHz, DMSO-d_6) δ 167.96 (2 × CO-NH), 136.99 (2 × Ar-X), 136.85 (2 × Ar-X), 128.32 (4 × Ar-H, CH_2 side), 118.98 (4 × Ar-H, NHAc side), 34.53 (2 × CH_2), 31.02 (2 × CH_2), 28.94 (CH_2), 28.82 (2 × CH_2), 28.57 (2 × CH_2), 23.92 (2 × CH_3-CO).

IR ν (cm^{-1}): 3297 (COHN); 2918, 2849 (CH_2); 1660 (CO); 1597, 1525 (Ar), 837 (*p*-disub. Ar).

I-3-7 1,7-Bis(4-phenylamine-4'-)heptane

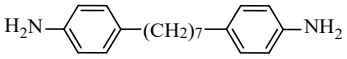

Synthesis procedure follows that described for **I-1** 1,5-bis(4-aminophenyl-4'-oxy)pentane

Quantities used: **i-3.2.7** (2.550 g, 6.958 mmol); EtOH (50 mL); NaOH (8.350 g, 0.209 mol) in H_2O (20 mL).

TLC indicated the complete consumption of **i-3.2** after 3 hours and the mono-hydrolysed product (not isolated) after 5 hours.

The crude product was used without further purification.

Yield: 1.836 g, 93%

m.p. = 82–84 ˚C

R_f (EtOAc) 0.58

^{1}H NMR (400 MHz, DMSO-d_6) δ 6.80 (d, J = 8.2 Hz, 4H, 4 × Ar-H), 6.46 (d, J = 8.3 Hz, 4H, 4 × Ar-H), 4.77 (s, 4H, 2 × NH_2), 2.36 (t, J = 7.6 Hz, 4H, 2 × Ar-$\underline{CH_2}$), 1.45 (quin, J =7.3 Hz, 4H, 2 × Ar-CH_2-$\underline{CH_2}$), 1.24 (m, 6H, 3 × CH_2).

^{13}C NMR (101 MHz, DMSO-d_6) δ 146.25 (2 × $\underline{Ar}$-NH_2), 129.28 (4 × Ar-H, CH_2 side), 128.55 (2 × $\underline{Ar}$-CH_2), 113.94 (4 × Ar-H, NH_2 side), 34.35 (2 × CH_2), 31.41 (2 × CH_2), 28.75 (CH_2), 28.60 (2 × CH_2).

IR ν (cm^{-1}): 3314, 3217 (Ar. NH_2); 2917, 2849 (CH_2); 1609, 1515 (Ar); 1267 (Ar. C-N); 826 (*p*-disub. Ar)

I-3-9 1,9-Bis(4-phenylamine-4'-)nonane

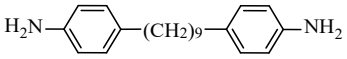

Synthesis procedure follows that described for **I-1** 1,5-bis(4-aminophenyl-4'-oxy)pentane

Quantities used: **i-3.2.9** (2.000 g, 5.069 mmol); EtOH (70 mL); NaOH (10.146 g, 0.254 mol) in H_2O (25 mL).

TLC indicated the complete consumption of **i-3.2.9** after 2 hours and the mono-hydrolysed product (not isolated) after 5 hours.

The crude product was used without further purification.

Yield: 1.237 g, 79%

m.p. = 97–102 ˚C

R_f (EtOAc) 0.81

^{1}H NMR (400 MHz, DMSO-d_6) δ 6.81 (d, J = 8.2 Hz, 4H, 4 × Ar-H), 6.46 (d, J = 8.3 Hz, 4H, 4 × Ar-H), 4.77 (s, 4H, 2 × NH_2), 2.37 (t, J = 7.6 Hz, 4H, 2 × Ar-$\underline{CH_2}$), 1.45 (quin, J = 7.0 Hz, 4H, 2 × Ar-CH_2-$\underline{CH_2}$), 1.35 – 1.14 (m, 10H, 5 × CH_2).

^{13}C NMR (101 MHz, DMSO-d_6) δ 146.25 (2 × $\underline{Ar}$-NH_2), 129.27 (4 × Ar-H, CH_2 side), 128.54 (2 × $\underline{Ar}$-CH_2), 113.93 (4 × Ar-H, NH_2 side), 34.37 (2 × CH_2), 31.43 (2 × CH_2), 29.02 (CH_2), 28.89 (2 × CH_2), 28.60 (2 × CH_2).

IR ν (cm^{-1}): 3396, 32316 (Ar. NH_2); 2916, 2848 (CH_2); 1625, 1515 (Ar); 1270 (Ar. C-N); 825 (*p*-disub. Ar)

2.3.2 Method 2

The methodology for the synthesis of **I-3-7** and **I-3-9** was previously described by Henderson *et al.* [2]

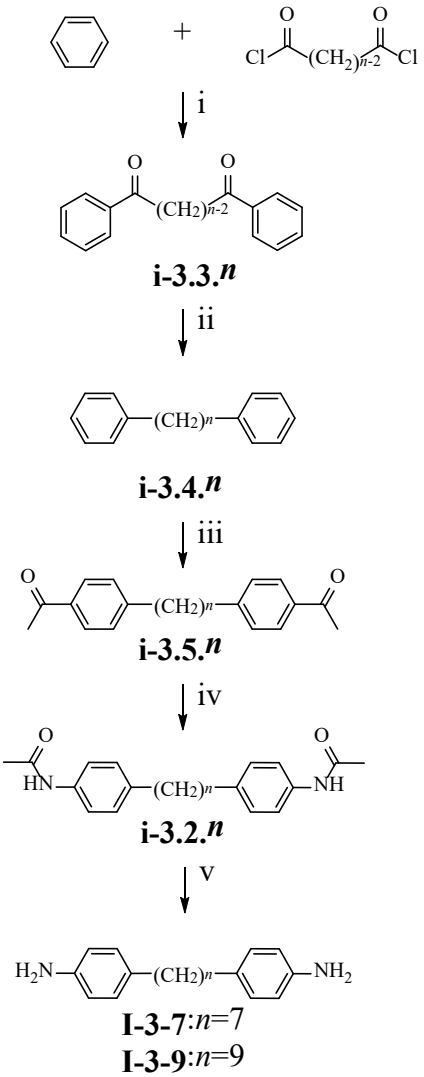

i) $AlCl_3$
ii) NH_2NH_2, KOH, diethylene glycol, 140 ^oC
iii) CH_3COCl, $AlCl_3$, DCM
iii) NaN_3, H_2SO_4, DCM
v) $NaOH_{(aq)}$, EtOH, 78 ^oC

Scheme 5: Synthetic route to form the *a,ω*-bis(4-aminophenyl-4'-)alkanes (**I-3-7** and **I-3-9**) by method 2.

i-3.3.7 1,7-Diphenylhepta-1,7-dione

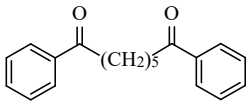

Yield: 73.53 g, 93%

^{1}H NMR (300 MHz, $CDCl_3$) δ 7.95 (m, 4H, 4 × Ar-H), 7.55 (m, 2H, 2 × Ar-H), 7.45 (m, 4H, 4 × Ar-H), 2.99 (t, *J* = 7.3 Hz, 4H, 2 × CO-$\underline{CH_2}$), 1.80 (quin, *J* = 7.6 Hz, 4H, 2 × CO-CH_2-$\underline{CH_2}$), 1.49 (m, 2H, CO-CH_2-CH_2-$\underline{CH_2}$).

^{13}C NMR (75 MHz $CDCl_3$) δ 200.21 (2 × $\underline{CO}$-Ar), 136.99 ($\underline{Ar}$-CO), 132.91 (2 × Ar-H), 128.55 (4 × Ar-H), 128.00 (4 × Ar-H), 38.30 (2 × CO-$\underline{CH_2}$), 28.95 (CO-CH_2-CH_2-$\underline{CH_2}$), 24.04 (2 × CO-CH_2-$\underline{CH_2}$).

IR ν (cm^{-1}): 2935 (C-H), 2850 (C-H), 1671 (C=O), 1597, 1477, 1406, 1360, 1281, 1231, 1208, 974, 960, 751, 688, 570, 454.

i-3.3.9 1,9-Diphenylnona-1,9-dione

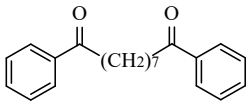

Yield: 24.45 g, 79 %

^{1}H NMR (300 MHz $CDCl_3$) δ 7.96 (m, 4H, 4 × Ar-H), 7.55 (m, 2H, 2 × Ar-H), 7.45 (m, 4H, 4 × Ar-H), 2.96 (t, *J* = 7.4 Hz, 4H, 2 × CO-$\underline{CH_2}$), 1.74 (quin, *J* = 7.6 Hz, 4H, 2 × CO-CH_2-$\underline{CH_2}$), 1.49 (m, 6H, 3 × CH_2).

^{13}C NMR (75 MHz $CDCl_3$) δ 200.64 (2 × $\underline{CO}$-Ar), 137.24 ($\underline{Ar}$-CO), 133.02 (2 × Ar-H), 128.70 (4 × Ar-H), 128.20 (4 × Ar-H), 38.70 (2 × CO-$\underline{CH_2}$), 29.46 (CH_2), 29.34 (CH_2), 24.42 (CH_2).

IR ν (cm^{-1}): 2937 (C-H), 2852 (C-H), 1674 (C=O), 1596, 1579, 1477, 1405, 1361, 1281, 1229, 1207, 974, 960, 751, 729, 688, 570, 432.

i-3.4.7 1,7-Diphenylheptane

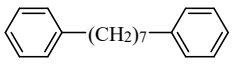

Yield: 16.91 g, 78%

^{1}H NMR (300 MHz $CDCl_3$) δ 7.28 (m, 4H, 4 × Ar-H), 7.19 (m, 6H, 6 × Ar-H), 2.61 (t, *J* = 7.5 Hz, 4H, 2 × Ar-$\underline{CH_2}$), 1.62 (quin, 4H, 2 × Ar-CH_2-$\underline{CH_2}$), 1.35 (m, 6H, 3 × CH_2).

^{13}C NMR (75 MHz $CDCl_3$) δ 142.94 (2 × $\underline{Ar}$-CH_2), 129.42 (4 × Ar-H), 128.22 (4 × Ar-H), 125.54 (2 × Ar-H), 35.98 (2 × Ar-$\underline{CH_2}$), 31.53 (CH_2), 29.49 (CH_2), 26.91 (CH_2).

IR ν (cm^{-1}): 2927 (C-H), 2852 (C-H), 1603, 1571, 1492, 1450, 1178, 1062, 1028, 746, 694, 570, 493.

i-3.4.9 1,9-Diphenylheptane

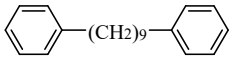

Yield: 21.01 g, 95 %

^{1}H NMR (300 MHz $CDCl_3$) δ 7.28 (m, 4H, 4 × Ar-H), 7.16 (m, 6H, 6 × Ar-H), 2.60 (t, *J* = 7.6 Hz, 4H, 2 × Ar-$\underline{CH_2}$), 1.55 (m, 4H, 2 × Ar-CH_2-$\underline{CH_2}$), 1.27 (m, 10H, 5 × CH_2).

^{13}C NMR (75 MHz $CDCl_3$) δ 142.95 (2 × $\underline{Ar}$-CH_2), 129.46 (4 × Ar-H), 128.22 (4 × Ar-H), 125.55 (2 × Ar-H), 35.99 (2 × Ar-$\underline{CH_2}$), 31.52 (CH_2), 29.49 (CH_2), 29.32 (CH_2), 26.91 (CH_2).

IR ν (cm^{-1}): 2925 (C-H), 2853 (C-H), 1600, 1570, 1495, 1450, 1179, 1064, 1028, 746, 692, 570, 493.

i-3.5.7 1,7-Bis(4-acetophenyl-1-)heptane

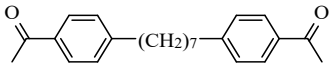

Yield: 22.15 g, 98 %

^{1}H NMR (300 MHz $CDCl_3$) δ 7.88 (d, *J* = 8.4 Hz, 4H, 2 × Ar-H), 7.26 (d, *J* = 8.4 Hz, 4H, 2 × Ar-H), 2.64 (t, *J* = 7.6 Hz, 4H, 2 × Ar-$\underline{CH_2}$), 2.59 (s, 6H, 2 × $\underline{CH_3}$-CO), 1.63 (m, 4H, 2 × CH_2), 1.32 (m, 6H, 3 × CH_2).

^{13}C NMR (75 MHz $CDCl_3$) δ 197.94 (2 × CO), 148.75 (2 × $\underline{Ar}$-CH_2), 134.88 (2 × $\underline{Ar}$-CO), 128.61 (4 × Ar-H), 128.47 (4 × Ar-H), 35.97 (2 × Ar-$\underline{CH_2}$), 31.11 (CH_2), 29.41 (2 × $\underline{CH_3}$-CO), 26.56 (CH_2), 24.29 (CH_2).

IR ν (cm^{-1}): 2931 (C-H), 2849 (C-H), 1680 (C=O), 1604, 1412, 1358, 1254, 1181, 958, 752, 690, 598, 579.

i-3.5.9 1,9-Bis(4-acetophenyl-1-)nonane

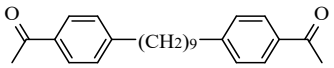

Yield: 24.6 g, 89 %

^{1}H NMR (300 MHz $CDCl_3$) δ 7.89 (d, *J* = 8.3 Hz, 4H, $\underline{Ar\text{-}H}$), 7.27 (d, *J* = 8.3 Hz, 4H, $\underline{Ar\text{-}H}$), 2.67 (t, *J* = 7.7 Hz, 4H, 2 × Ar-$\underline{CH_2}$), 2.60 (s, 6H, 2 × $\underline{CH_3}$-CO), 1.61 (m, 4H, 2 × Ar-CH_2-$\underline{CH_2}$), 1.33 (m, 14H, 7 × CH_2).

^{13}C NMR (75 MHz $CDCl_3$) δ 197.92 (2 × CO), 148.79 (2 × $\underline{Ar}$-CH_2), 134.91 (2 × $\underline{Ar}$-CO), 128.61 (4 × Ar-H), 128.48 (4 × Ar-H), 35.98 (2 × Ar-$\underline{CH_2}$), 31.11 (CH_2), 29.42 (2 × $\underline{CH_3}$-CO), 29.22 (CH_2), 26.57 (CH_2), 24.29 (CH_2).

IR ν (cm^{-1}): 2926 (C-H), 2854 (C-H), 1679 (C=O), 1605, 1411, 1357, 1266, 1181, 956, 752, 691, 597, 581.

i-3.2.7 1,7-Bis(4-phenylacetamide-4'-)heptane

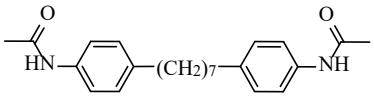

Yield: 2.28 g, 12 %

^{1}H NMR (300 MHz $CDCl_3$) δ 7.52 (s, 2H, 2 × Ac-NH), 7.36 (d, *J* = 8.4 Hz, 4H, 4 × Ar-H), 7.12 (d, *J* = 8.3 Hz, 4H, 4 × Ar-H), 2.54 (t, *J* = 7.6 Hz, 4H, 2 × Ar-CH_2), 2.17 (s, 6H, 2 × CH_3-CO), 1.60 (m, 4H, 2 × Ar-CH_2-CH_2), 1.30 (m, 6H, 3 × CH_2).

^{13}C NMR (75 MHz $CDCl_3$) Relative insolubility of the compound precluded the possibility of ^{13}C NMR spectroscopy.

IR ν (cm^{-1}): 3301 (CONH), 2917 (C-H), 2847 (C-H), 1656, 1600, 1543, 1516, 1440, 1310, 1252, 1064, 821, 751, 721, 691, 602, 511.

i-3.2.9 1,9-Bis(4-phenylacetamide-4'-)nonane

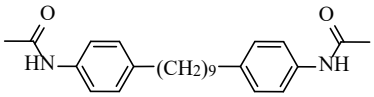

Yield: 15.16 g, 58 %

^{1}H NMR (300 MHz $CDCl_3$) δ 7.50 (s, 2H, 2 × Ac-NH), 7.37 (d, *J* = 8.3 Hz, 4H, 4 × Ar-H), 7.10 (d, *J* = 8.2 Hz, 4H, 4 × Ar-H), 2.55 (t, *J* = 7.7 Hz, 4H, 2 × Ar-CH_2), 2.17 (s, 6H, 2 × CH_3-CO), 1.60 (m, 4H, 2 × Ar-CH_2-CH_2), 1.30 (m, 10H, 5 × CH_2).

^{13}C NMR (75 MHz $CDCl_3$) Relative insolubility of the compound precluded the possibility of ^{13}C NMR spectroscopy.

IR ν (cm^{-1}): 3302 (CONH), 2916 (C-H), 2848 (C-H), 1659, 1598, 1544, 1516, 1440, 1409, 1316, 1252, 1066, 822, 751, 721, 691, 603, 509.

I-3-7 1,7-Bis(4-phenylamine-4'-)heptane

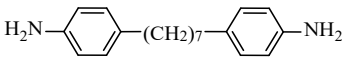

Yield: 0.70 g, 44 %

^{1}H NMR (300 MHz $CDCl_3$) δ 6.97 (d, *J* = 8.2 Hz, 4H, 4 × Ar-H), 6.63 (d, *J* = 8.2 Hz, 4H, 4 × Ar-H), 3.57 (s, 4H, 2 × NH_2) 2.42 (t, *J* = 7.8 Hz, 4H, 2 × Ar-$\underline{CH_2}$), 1.53 (quin, *J* = 7.3 Hz, 4H, 2 × Ar-CH_2-$\underline{CH_2}$), 1.27 (m, 6H, 3 × CH_2).

^{13}C NMR (75 MHz $CDCl_3$) δ 143.97 (2 × Ar-NH_2), 133.14 (2 × Ar-CH_2), 129.19 (4 × Ar-H), 115.18 (4 × Ar-H), 35.09 (2 × CH_2), 31.89 (CH_2), 29.56 (CH_2), 29.27 (CH_2).

IR ν (cm^{-1}): 3317 (NH_2), 2927 (C-H), 2849 (C-H), 1596, 1511, 1458, 1310, 1263, 1153, 1107, 1025, 888, 825, 721, 548, 532.

I-3-9 1,9-Bis(4-phenylamine-4'-)nonane

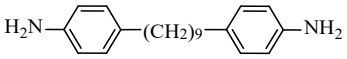

Yield: 0.38 g, 4 %

^{1}H NMR (300 MHz $CDCl_3$) δ 6.96 (d, *J* = 8.3 Hz, 4H, 4 × Ar-H), 6.62 (d, *J* = 8.4 Hz, 4H, 4 × Ar-H), 3.54 (s, 4H, 2 × NH_2) 2.48 (t, *J* = 7.7 Hz, 4H, 2 × Ar-$\underline{CH_2}$), 1.53 (quin, *J* = 7.4 Hz, 4H, 2 × Ar-CH_2-$\underline{CH_2}$), 1.26 (m, 10H, 5 × CH_2).

^{13}C NMR (75 MHz $CDCl_3$)δ: 143.98 (2 × Ar-NH_2), 133.15 (2 × Ar-CH_2), 129.15 (4 × Ar-H), 115.20 (4 × Ar-H), 35.08 (CH_2), 31.84 (CH_2), 29.56 (CH_2), 29.53 (CH_2), 29.28 (CH_2).

IR ν (cm^{-1}): 3313 (NH_2), 2930 (C-H), 2850 (C-H), 1599, 1571, 1511, 1458, 1309, 1253, 1163, 1106, 1026, 886, 825, 720, 566, 548, 532.

2.4 Benzylideneaniline-Based Dimers

The synthesis of the dimers X-O5O-X, X-6O-X, X-7-X and X-9-X follow Scheme 6. The synthetic procedure for CN.6O.CN is described in detail as a representative example for all dimer syntheses, and the reaction conditions for the synthesis of representative liquid crystal dimers are given in Table 1.

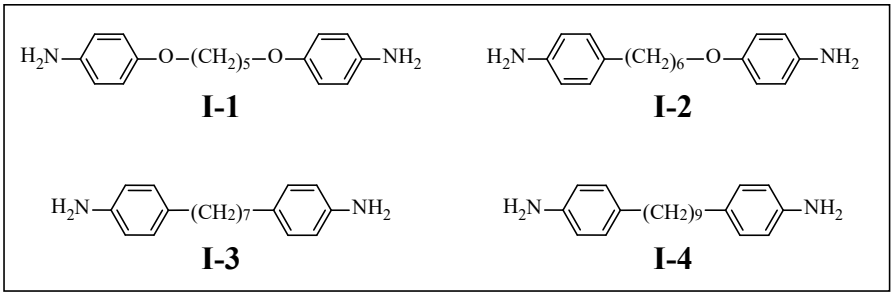

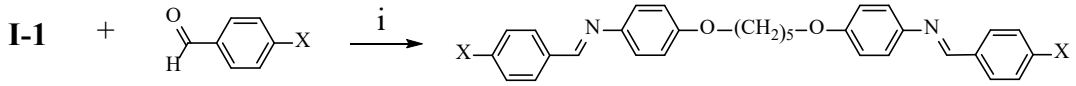

X=CN: CN-O5O-CN

X=OC_mH_{2m+1}: *m*O-O5O-O*m*, *m*=1-9

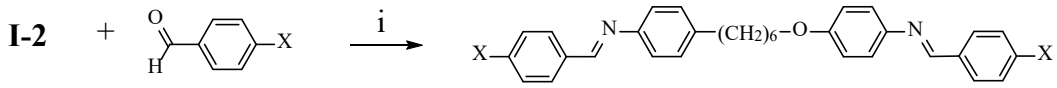

X=CN: CN-6O-CN

X=OC_mH_{2m+1}: *m*O-6O-O*m*, *m*=1-9

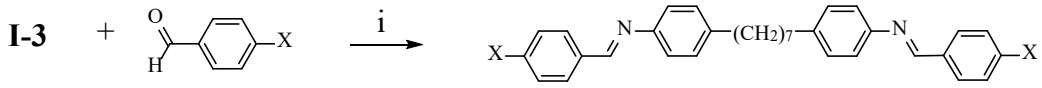

X=CN: CN-7-CN

X=OC_mH_{2m+1}: *m*O-7-O*m*, *m*=1-9

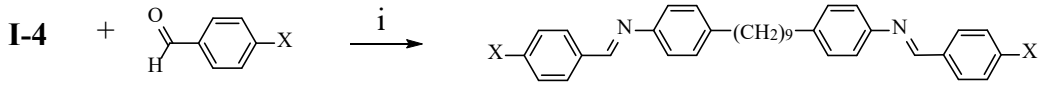

X=CN: CN-9-CN

X=OC_mH_{2m+1}: *m*O-9-O*m*, *m*=1-6

i) *p*-TSOH, EtOH

Scheme 6: Synthetic route to form the target liquid crystal dimers.

After the complete dissolution of **I-2** (0.150 g, 0.527 mmol) by heating in EtOH (20 mL) to 78 °C, 4-cyanobenzaldehyde (0.138 g, 1.055 mmol) was added in one portion, followed by a crystal of *p*-toluenesulfonic acid. The reaction was stirred at 78 °C for 5 hours, cooled to room temperature before the resultant precipitate was collected. The crude product was purified by recrystallisation from EtOH (15 mL) to give the title compound as a white powder.

Table 1: Reaction conditions for the synthesis of liquid crystal dimers CN-O5O-CN, CN-6O-CN, CN-7-CN, CN-9-CN, 1O-O5O-O1, 1O-6O-O1, 1O-7-O1 and 1O-9-O1.

Compound	**I-** mass / g (moles / mmol)	4-cyanobenzaldehyde mass / g (moles / mmol)		Reaction time / hr	Recrystallisation solvent volume / mL
CN-O5O-CN	**I-1** 0.200 (0.698)	0.229 (1.745)		5.0	20
CN-6O-CN	**I-2** 0.150 (0.527)	0.138 (1.055)		5.0	15
CN-7-CN	**I-3-7** 0.207 (0.733)	0.234 (1.784)		3.0	30
CN-9-CN	**I-3-9** 0.155 (0.499)	0.148 (1.129)		4.0	20
	I- mass / g (moles / mmol)	4-methoxybenzaldehyde mass / g (moles / mmol)	volume /mL	Reaction time / hr	Recrystallisation solvent volume / mL
1O-O5O-O1	**I-1** 0.200 (0.698)	0.285 (2.094)	0.26	16.0	15
1O-6O-O1	**I-2** 0.150 (0.527)	0.144 (1.055)	0.13	7.0	15
1O-7-O1	**I-3-7** 0.111 (0.393)	0.190 (1.397)	0.17	3.0	30
1O-9-O1	**I-3-9** 0.094 (0.303)	0.112 (0.823)	0.10	4.0	20

Purification by recrystallisation from EtOH.

CN-O5O-CN

Yield: 0.126 g, 35 %

^{1}H NMR (300 MHz, $CDCl_3$) δ 8.52 (s, 2H, 2 × CH=N), 7.99 (d, *J* = 8.4 Hz, 4H, 4 × Ar-H), 7.74 (d, *J* = 8.3 Hz, 4H, 4 × Ar-H), 7.28 (d, *J* = 9.0 Hz, 4H, 4 × Ar-H), 6.95 (d, *J* = 8.9 Hz, 4H, 4 × Ar-H), 4.03 (t, *J* = 6.3 Hz, 4H, CH_2-O), 1.90 (quin , *J* = 6.6 Hz, 4H, CH_2-CH_2-O), 1.76 – 1.63 (m, 2H, CH_2).

^{13}C NMR (75 MHz, $CDCl_3$) δ 158.71, 155.41, 143.70, 140.42, 132.64, 128.95, 122.68, 118.71, 115.19, 114.05, 68.15, 29.17, 22.90.

CN-6O-CN

Yield: 0.198 g, 74 %

^{1}H NMR (400 MHz, $CDCl_3$) δ 8.51 (s, 2H, 2 × CH=N), 8.04 – 7.94 (2 × d overlapping (observed as m), 4H, 4 × Ar-H), 7.75 (d, *J* = 8.7 Hz, 4H, 4 × Ar-H), 7.27 (d, *J* = 9.3 Hz, 2H, 2 × Ar-H), 7.23 (d, *J* = 8.2 Hz, 2H, 2 × Ar-H), 7.19 (d, *J* = 8.1 Hz, 2H, 2 × Ar-H), 6.93 (d, *J* = 8.5 Hz, 2H, 2 × Ar-H), 3.98 (t, *J* = 6.5 Hz, 2H, CH_2-O), 2.66 (t, *J* = 7.7 Hz, 2H, CH_2-Ar), 1.81 (quin, *J* = 6.9 Hz, 2H, CH_2-CH_2-O), 1.69 (quin, *J* = 7.6 Hz, 2H, CH_2), 1.59 – 1.48 (m, 2H, CH_2), 1.48 – 1.38 (m, 2H, CH_2).

^{13}C NMR (101 MHz, $CDCl_3$) δ 158.81, 157.06, 155.34, 148.75, 143.65, 141.98, 140.46, 140.27, 132.65, 132.64, 129.42, 129.13, 128.94, 122.67, 121.12, 118.70, 118.64, 115.21, 114.35, 114.08, 68.33, 35.57, 31.50, 29.33, 29.08, 26.06.

Elemental analysis: Calculated %: C 79.97, H 5.92, N 10.97. Found %: C 79.77, H 5.93, N 10.71.

CN-7-CN

Yield: 0.100 g, 38 %

^{1}H NMR (300 MHz, $CDCl_3$) δ 8.74 (s, 2H, 2 × CH=N), 8.09 (d, *J* = 5.9 Hz, 4H, 4 × Ar-H), 7.97 (d, *J* = 7.5 Hz, 4H, 4 × Ar-H), 6.85 (d, *J* = 7.8 Hz, 4H, 4 × Ar-H), 6.53 (d, *J* = 7.6 Hz, 4H, 4 × Ar-H), 2.59 (t, *J* = 7.0 Hz, 4H, 2 × CH_2-Ar), 1.57 (m, 4H, 2 × CH_2), 1.31 (m, 6H, 3 × CH_2).

IR (cm^{-1}): 2924 (C-H), 2849 (C-H), 2224 (C≡N), 1624, 1502, 1462, 1366, 1191, 836, 727, 555.

Elemental analysis: Calculated %: C 82.64, H 6.34, N 11.01. Found %: C 82.22, H 6.42, N 10.76.

MS (ESI^+, m/z): $[M^+Na]^+$ Calculated for $C_{35}H_{32}N_4Na$: 531.2525. Found: 531.2505.

CN-9-CN

Yield: 0.050 g, 18 %

^1H NMR (300 MHz $CDCl_3$) δ 8.51 (s, 2H, 2 × CH=N), 8.00 (d, *J* = 8.2 Hz, 4H, 4 × Ar-H), 7.76 (d, *J* = 8.2 Hz, 4H, 4 × Ar-H), 7.23 (d, *J* = 8.6 Hz, 4H, 4 × Ar-H), 7.18 (d, *J* = 8.6 Hz, 4H, 4 × Ar-H), 2.63 (t, *J* = 7.6 Hz, 4H, 2 × CH_2-Ar), 1.64 (m, 4H, 2 × CH_2), 1.36 (m, 10H, 5 × CH_2).

^{13}C NMR (75 MHz $CDCl_3$) δ 157.06, 148.66, 142.18, 140.25, 132.67, 129.41, 129.13, 121.09, 118.67, 114.32, 35.65, 31.59, 29.47, 29.31.

IR (cm^{-1}): 2921 (C-H), 2849 (C-H), 2229 (C≡N), 1624, 1506, 1466, 1362, 1194, 885, 841, 723, 557, 534.

Elemental analysis: Calculated %: C 82.80, H 6.76, N 10.44. Found %: C 82.75, H 6.94 N 10.27.

MS (ESI^+, m/z): $[M^+Na]^+$ Calculated for $C_{37}H_{36}N_4Na$: 559.2838. Found: 559.2828.

1O-O5O-O1

Yield: 0.206 g, 57 %

^1H NMR (400 MHz, $CDCl_3$) δ 8.41 (s, 2H, 2 × CH=N), 7.83 (d, *J* = 8.4 Hz, 4H, 4 × Ar-H), 7.19 (d, *J* = 8.5 Hz, 4H, 4 × Ar-H), 6.97 (d, *J* = 8.4 Hz, 4H, 4 × Ar-H), 6.92 (d, *J* = 8.5 Hz, 4H, 4 × Ar-H), 4.02 (t, *J* = 6.4 Hz, 4H, CH_2-O), 3.87 (s, 6H, CH_3-O), 1.89 (quin, *J* = 7.0, 6.3 Hz, 4H, -CH_2-CH_2-O), 1.68 (quin, *J* = 7.2 Hz, 2H, -CH_2-CH_2-CH_2-O).

^{13}C NMR (101 MHz, $CDCl_3$) δ 162.11, 157.95, 157.59, 145.33, 130.37, 129.67, 122.20, 115.12, 114.29, 77.48, 77.16, 76.84, 68.18, 55.57, 29.24, 22.91.

IR (cm^{-1}): 2930 (C-H), 1621, 1606, 1574, 1509, 1468, 1418, 1303, 1236, 1194, 1167, 111, 839 (*p*-disub. Ar)

1O-6O-O1

Yield: 0.176 g, 64 %

^{1}H NMR (400 MHz, $CDCl_3$) δ 8.40 (s, 2H, 2 × CH=N), 7.89 – 7.77 (2 × d overlapping (observed as m), 4H, 4 × Ar-H), 7.19 (d, *J* = 8.2 Hz, 4H, 4 × Ar-H), 7.13 (d, *J* = 7.9 Hz, 2H, 2 × Ar-H), 6.97 (d, *J* = 8.2 Hz, 4H, 4 × Ar-H), 6.91 (d, *J* =8.4 Hz, 2H, 2 × Ar-H), 3.97 (t, *J* = 6.5 Hz, 2H, CH_2-O), 3.87 (s, 4H, 2 × CH_3-O), 2.64 (t, *J* = 7.7 Hz, 2H, CH_2-Ar), 1.80 (quin, *J* = 6.8 Hz, 2H, -CH_2-CH_2-O), 1.68 (quin, *J* = 7.7 Hz, 2H, -CH_2-CH_2-CH_2-O), 1.56 – 1.47 (m, 2H, CH_2), 1.47 – 1.36 (m, 2H, CH_2).

^{13}C NMR (101 MHz, $CDCl_3$) δ 162.24, 162.09, 159.10, 157.88, 157.66, 150.12, 145.24, 140.35, 130.53, 130.36, 129.69, 129.58, 129.22, 122.19, 120.94, 115.11, 114.29, 114.28, 68.31, 55.56, 35.51, 31.56, 29.38, 29.08, 26.06.

Elemental analysis: Calculated %: C 78.43, H 6.97, N 5.38. Found %: C 78.36, H 6.94, N 5.30.

1O-7-O1

Yield: 0.06 g, 28%

^{1}H NMR (300 MHz $CDCl_3$) δ 8.40 (s, 2H, 2 × CH=N), 7.84 (d, *J* = 8.8 Hz, 4H, 4 × Ar-H), 7.19 (d, *J* = 8.4 Hz, 4H, 4 × Ar-H), 7.13 (d, *J* = 8.4 Hz, 4H, 4 × Ar-H), 6.98 (d, *J* = 8.8 Hz, 4H, 4 × Ar-H), 3.87 (s, 6H, 2 × CH_3-O), 2.61 (t, *J* = 7.5 Hz, 4H, 2 × CH_2-Ar), 1.62 (m, 4H, 2 × CH_2), 1.34 (m, 6H, 3 × CH_2).

^{13}C NMR (75 MHz $CDCl_3$) δ 162.24, 159.07, 150.07, 140.56, 130.53, 129.60, 129.21, 120.92, 114.29, 55.57, 35.60, 31.63, 29.47, 29.30.

IR (cm^{-1}): 2914 (C-H), 2847 (C-H), 1624, 1603, 1573, 1510, 1467, 1307, 1250, 1166, 1166, 1029, 836, 545.

Elemental analysis: Calculated %: C 81.05, H 7.38, N 5.40. Found %: C 81.12, H 7.67, N 5.44.

MS (ESI^+, m/z): $[M^+H]^+$ Calculated for $C_{35}H_{39}N_2O_2$: 519.3012. Found: 519.3002.

1O-9-O1

Yield: 0.022 g, 14 %

^{1}H NMR (300 MHz $CDCl_3$) δ 8.40 (s, 2H, 2 × CH=N), 7.84 (d, *J* = 8.8 Hz, 4H, 4 × Ar-H), 7.19 (d, *J* = 8.4 Hz, 4H, 4 × Ar-H), 7.13 (d, *J* = 8.4 Hz, 4H, 4 × Ar-H), 6.98 (d, *J* = 8.8 Hz, 4H, 4 × Ar-H), 3.87 (s, 6H, 2 × CH_3-O), 2.63 (t, *J* = 7.6 Hz, 4H, 2 × CH_2-Ar), 1.60 (m, 4H, 2 × CH_2), 1.30 (m, 10H, 5 × CH_2).

^{13}C NMR (75 MHz $CDCl_3$) δ 162.24, 158.97, 150.07, 140.56, 130.39, 129.60, 129.08, 120.77, 114.14, 55.44, 35.49, 31.63, 29.64, 29.45, 29.27.

IR (cm^{-1}): 2930 (C-H), 2850 (C-H), 1593, 1571, 1511, 1458, 1309, 1253, 1163, 1106, 1026, 886, 825, 720, 566, 548, 532.

Elemental analysis: Calculated %: C 81.28, H 7.74, N 5.12. Found %: C 81.34, H 7.88, N 5.28.

MS (ESI^+, m/z): $[M^+H]^+$ Calculated for $C_{37}H_{43}N_2O_2$: 547.3325. Found: 547.3317.

Section 3: References

1. Henderson PA, Inkster RT, Seddon JM, Imrie CT. Highly non-linear liquid crystal tetramers. J Mater Chem. 2001;11:2722-31.

2. Henderson PA, Niemeyer O, Imrie CT. Methylene-linked liquid crystal dimers. Liq Cryst. 2001;28:463-72.